PHILOSOPHICAL TRANSACTIONS OF THE ROYAL SOCIETY A MATHEMATICAL, PHYSICAL & ENGINEERING SCIENCES

Solution of Laplace's Equations for the M$_{2}$ Tide in the World Oceans

C. L. Pekeris and Y. Accad

Phil. Trans. R. Soc. Lond. A 1969 **265**, 413-436
doi: 10.1098/rsta.1969.0062

SOLUTION OF LAPLACE'S EQUATIONS FOR THE M_2 TIDE IN THE WORLD OCEANS

By C. L. PEKERIS and Y. ACCAD
Department of Applied Mathematics, The Weizmann Institute, Rehovot, Israel

(*Communicated by Sir Harold Jeffreys F.R.S.—Received* 4 *December* 1968—
Revised 14 *February* 1969)

[Coloured map, pull-out facing p. 436]

CONTENTS

Laplace's tidal equations were solved for the M_2 tide in a realistic model of the world oceans based on the observed topography of the ocean bottom. When friction was neglected, the theoretical tides came out high, but of the right order of magnitude. The tidal heights proved to be sensitive to changes in the configuration of the coastline, indicating a state of near resonance. However, the positions of the amphidromic centres remained stable and were located close to the empirically deduced amphidromes. A fine computational grid was required to assure numerical convergence of the solution.

A solution was also carried out with friction included, on the assumption of a bottom frictional force proportional to the first power of the velocity. For a coefficient of friction appropriate to tidal currents in shallow waters, the theoretical tidal heights came out in fair agreement with the observed values. With friction included, the solution proved insensitive to changes in the configuration of the coastline, and the numerical convergence was also improved. The resulting rate of tidal dissipation was higher than the observationally deduced values, but the excess is within the uncertainty of the latter.

Our solution for the M_2 tide is given in figure 10, and the corresponding tidal current chart in figure 12. Figure 11 gives a comparison of the Middle South Atlantic amphidrome, which was derived from theory, with tidal observations in island stations.

Vol. 265. A. 1165. (Price 17*s*.; U.S. $2.20) 41 [Published 18 December 1969

1. Introduction

From Laplace's tidal equations, which date back to the year 1775, and from the known tidal potential and the topography of the ocean bottom, it should be possible to determine the tide theoretically at every point inside and on the coasts of the real world oceans, without having recourse to tidal observations at all. In this paper we present the results of the first phase of such an investigation. The aim in this phase was, in the first instance, to develop suitable numerical methods for handling a system of linear equations involving some 50 000 unknowns. The unknowns are the amplitudes and phases of the two components of velocity at each grid-point in the ocean. With our computer Golem, which is of the 'third generation' class, we have been able to come down to a grid-size of only 1° in latitude and longitude. The ocean was delineated to the same degree of fineness, as shown in figures 1 and 10.

In the original Laplace's tidal equations, friction was neglected entirely. Since the frictional forces are quadratic in the tidal velocities, which would complicate the calculations considerably, we limited ourselves initially to a frictionless ocean, and the results are presented in § 2. Given an ocean model in which the coastline is defined by arcs of length K in longitude and latitude, and a solution of the tidal equations obtained for this model in which a computational grid k ($\leqslant K$) was used, the first question that we investigated was how small k has to be taken in order to assure convergence (as k is decreased) of the finite-difference scheme to the solution of the tidal differential equations. By carrying out a solution with k halved, we found that in the case of an ocean bounded by a 'smooth' coastline (figures 3, 4), k can be taken as large as K. In the case of an ocean model defined by a 'rough' coastline (figures 5, 6), k must be reduced to $\frac{1}{2}K$ or less in order to ensure numerical convergence.

The second question that arose is how sensitive the theoretical tides are to changes in the configuration of the coastline, assuming, of course, that in each case an adequate value of the computational grid k was used to assure numerical convergence. In the case of the frictionless ocean models, we found that the theoretical tides are sensitive to changes in the coastal configuration, as shown in table 2 and in figures 2 and 3. This points to a state of near-resonance for the M_2 tide. On the other hand, the positions of the amphidromic systems turned out to be relatively stable (figure 7 and table 1), in spite of the large variations in tidal amplitudes between the various models.

The neglect of tidal friction thus leads to slow numerical convergence and, in addition, yields tidal values which on the one hand are too large in comparison with the observed values, and on the other hand are sensitive to the details of the coastal configuration. It appeared therefore that inclusion of tidal friction cannot be avoided. Section 3 presents our solution of Laplace's tidal equations when friction is included. In this investigation, we made the simplifying assumption that the bottom frictional force is proportional to the first power of the velocity (equation (4)), rather than to the second (equation (3)), which is required both by experiment and by geophysical observations. However, once the solution based on the linear friction law is available, it appears to be feasible to achieve a solution also for the square law, and we plan to carry out such a solution in the second phase of this work.

It turns out that, with an assumed linear law, the frictional effect appears in the tidal equations (17) and (18) only through the single factor $(1-i\gamma)$, which has the value 1 in the case of no friction. We have found that the effect of friction becomes significant after γ reaches a value of about 0.5 near the coast. In this calculation we have let γ decrease from the coast inversely as

the second power (instead of the first) of the ocean depth (equation (20)), in order to minimize the effect of friction in the interior of the ocean. In our ocean model there is no shelf, and the coast is essentially the 1 km depth contour, at which depth frictional effects in the real ocean are effectively small. However, the value of γ adopted gives us a frictional force near the coast in our model of the same order of magnitude as is found near the shallower coast in the real ocean.

The tidal solutions obtained for the ocean with friction included gave the following results:

(*a*) Even for an ocean model with a rough coastline, the solutions were stable as the computational grid k was reduced (compare figure 8 with figure 9).

(*b*) The solutions were insensitive to moderate changes in the configuration of the coastline (compare figure 9 with figure 10).

(*c*) The tidal amplitudes came out of the right order of magnitude when compared with the observed values.

(*d*) Even when friction is included, the phases of the tides were still somewhat advanced relative to the observed values.

(*e*) The rate of tidal dissipation by friction in the ocean came out about twice the value of 3 TJ/s† deduced by Munk & MacDonald from the observed acceleration of the Moon. The latter is, however, uncertain, possibly by a factor of 2, since Jeffreys deduces a value from the observations which is half as large.

The indicated state of near-resonance to the M_2 tide in the absence of friction prompts the speculation that in geologic history only those configurations of the ocean bottom had permanence, and were not subjected to violent erosion by tidal currents, which provided sufficient shelf area to generate the frictional forces required for the damping of the tides.

In the matter of comparison of observed tides with our theoretical values, we confine ourselves at this stage mainly to one point, discussed in § 5, which is the question of the reality of the Middle South Atlantic amphidrome shown in figure 10. This amphidrome has not appeared in any of the empirical tidal charts published hitherto. Using data for island stations, we show in figure 11 and in table 3 that the observations tend to support the existence of this amphidrome.

The tidal current chart for our solution given in figure 10, is shown in figure 12. We note that at the positions of the amphidromic centres, the tidal currents do not vanish, like the tidal elevation, but have a normal value.

2. Solution of Laplace's tidal equations for a frictionless ocean

(*a*) *Topography of the ocean bottom*

In this investigation, we have solved Laplace's tidal equations for the real world oceans, including a frictional term. Since the variable depth of the ocean bottom $h(\theta, \lambda)$ enters in Laplace's equations, we had, as a first step, to decide on a model of the ocean which would represent as closely as possible the real depths and the actual shape of the coastline.

The finest model we have dealt with so far is a '1° ocean', in which the coastline is defined by arcs of 1 degree in longitude and in latitude, as shown in figure 1. In this map we have drawn the contour lines of equal depth in steps of 500 m. The coastline is essentially the 1 km contour line. This map is of a preliminary nature, and is intended only for the purpose of testing our numerical solution, rather than as a definitive chart. It is based on data taken from the

† $1\,\mathrm{TJ} = 10^{12}\,\mathrm{J} = 10^{19}$ erg.

PHILOSOPHICAL TRANSACTIONS OF THE ROYAL SOCIETY A MATHEMATICAL, PHYSICAL & ENGINEERING SCIENCES

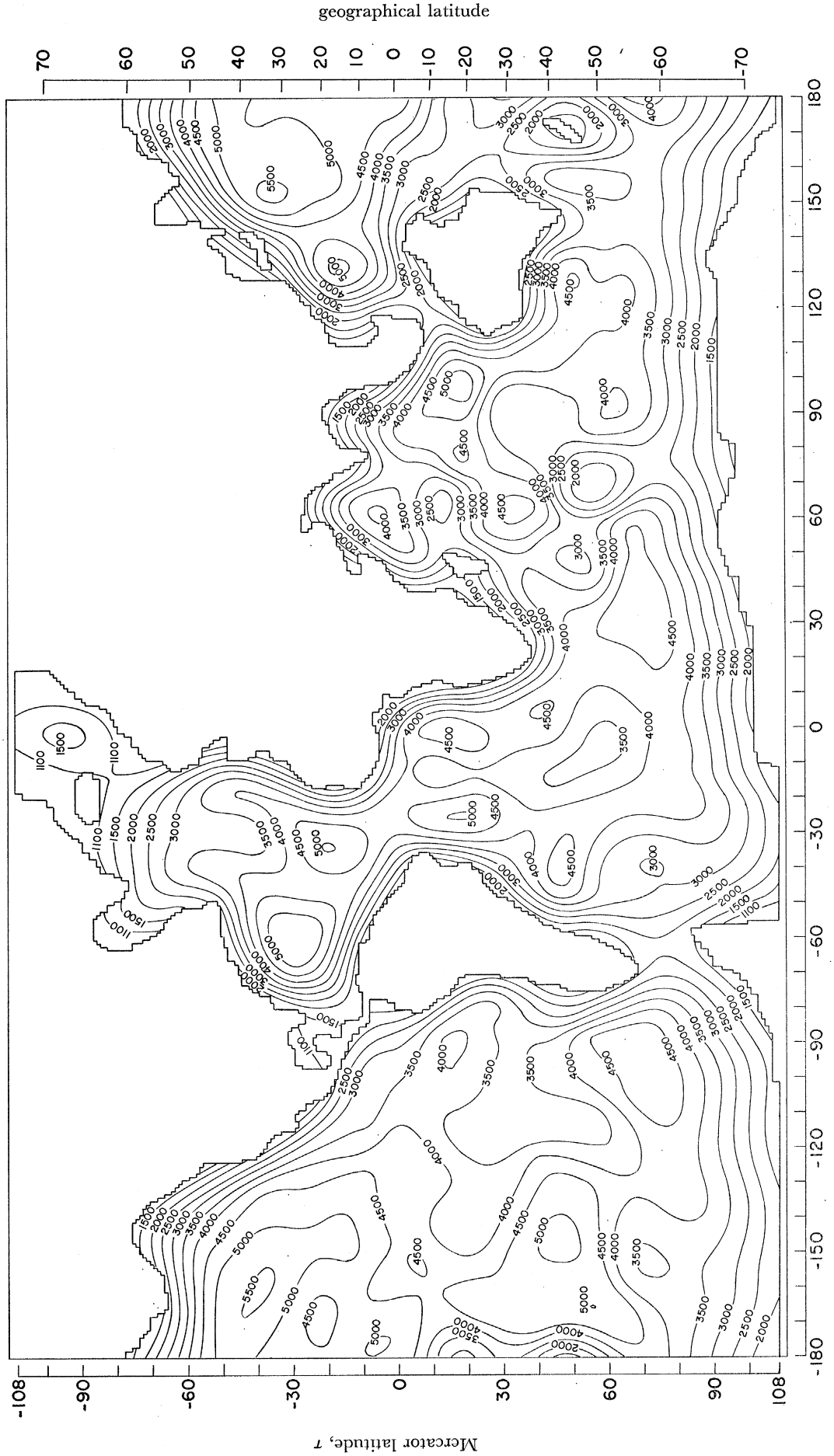

FIGURE 1. Map 1° *A*. Contour lines of depths of world oceans in metres.

PHILOSOPHICAL TRANSACTIONS OF THE ROYAL SOCIETY A MATHEMATICAL, PHYSICAL & ENGINEERING SCIENCES

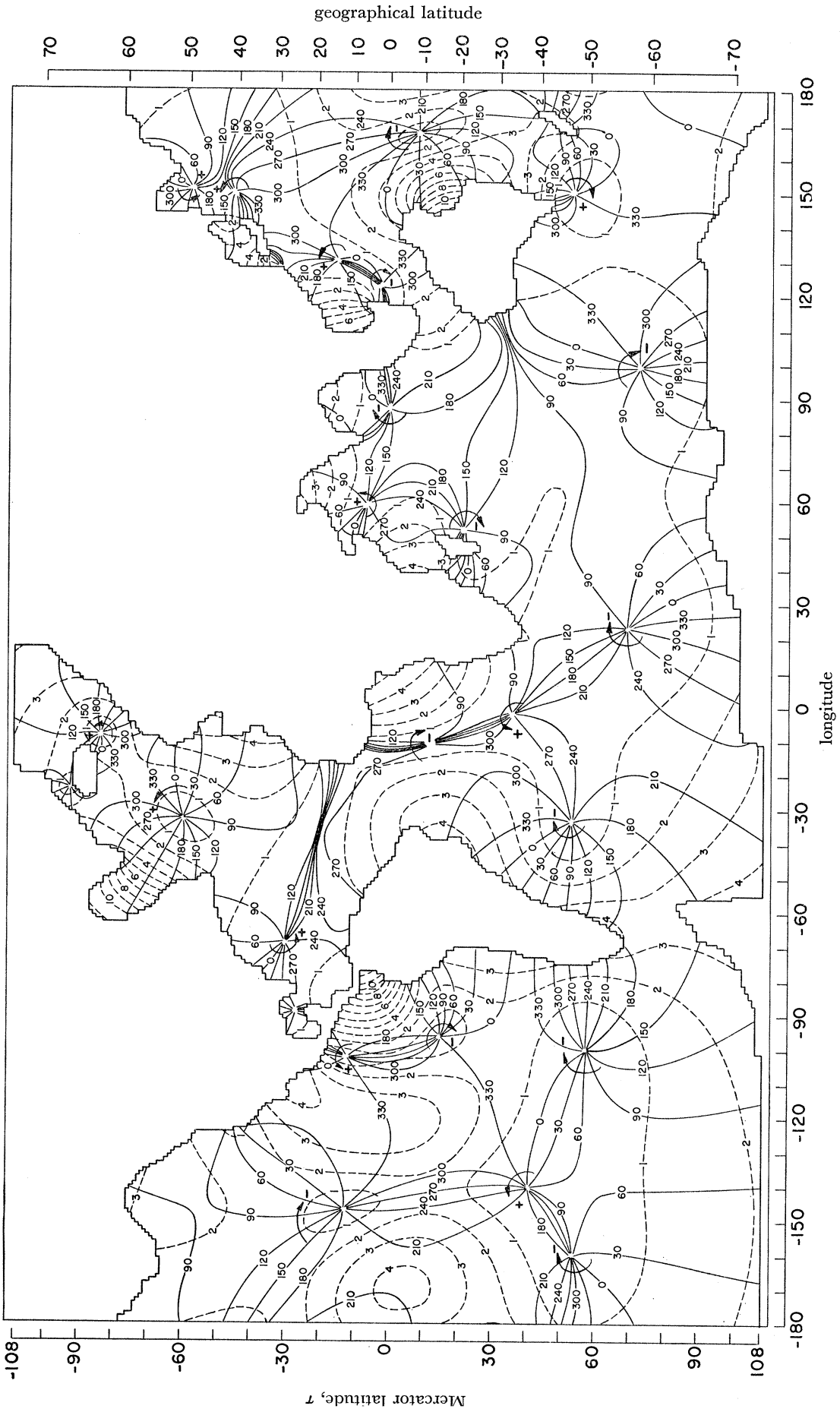

FIGURE 2. Cotidal lines (——) and corange lines (metres) (– – –) for the M_2 tide. Map 1° A; computation grid $k = 1.0°$.

PHILOSOPHICAL TRANSACTIONS OF THE ROYAL SOCIETY A MATHEMATICAL, PHYSICAL & ENGINEERING SCIENCES

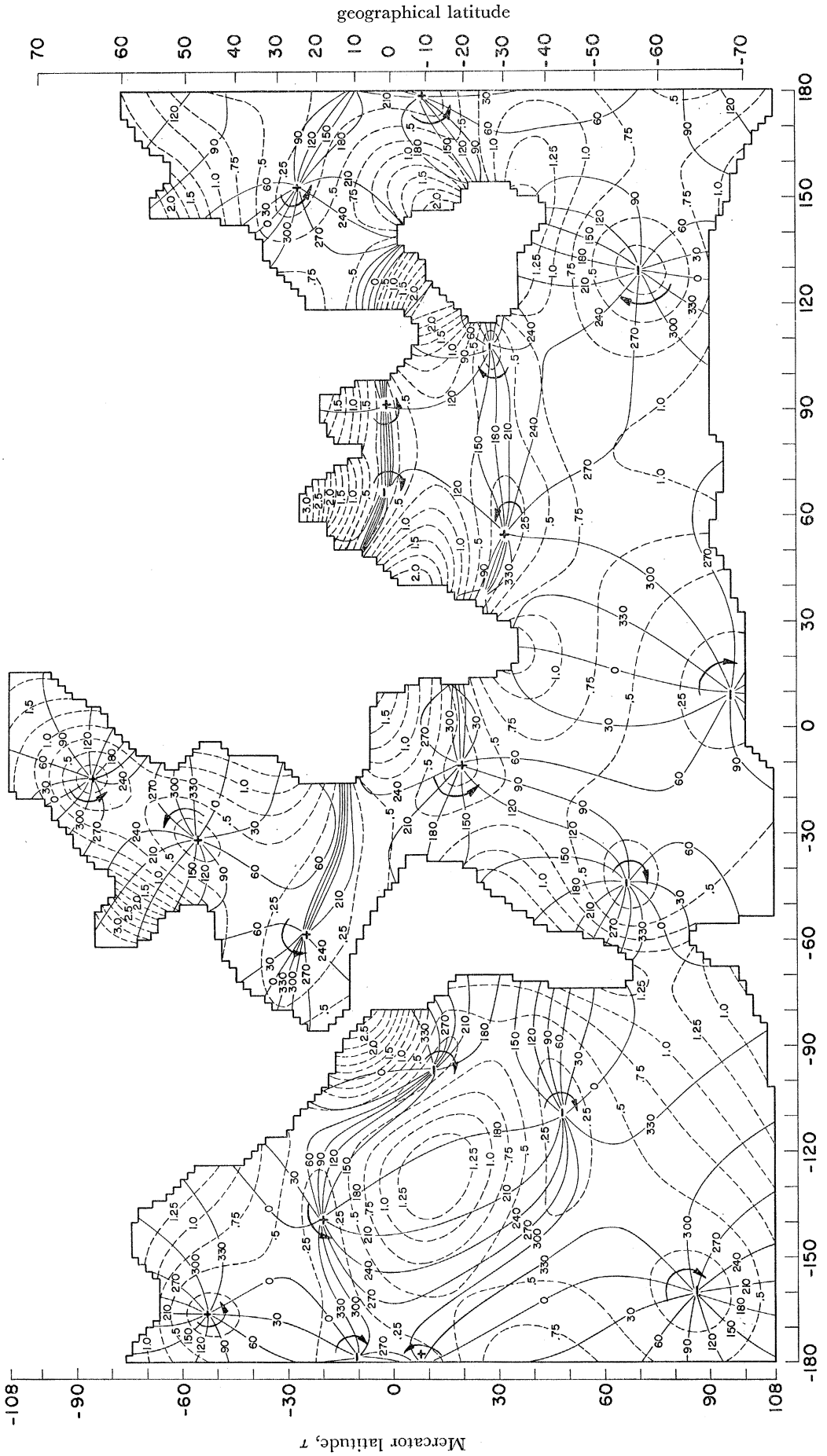

FIGURE 3. Cotidal lines (——) and corange lines (metres) (– – –) for the M_2 tide. Map 2° A; computation grid $k = 2°$; $f = \sigma/2\omega = 0.9635$.

PHILOSOPHICAL TRANSACTIONS OF THE ROYAL SOCIETY A MATHEMATICAL, PHYSICAL & ENGINEERING SCIENCES

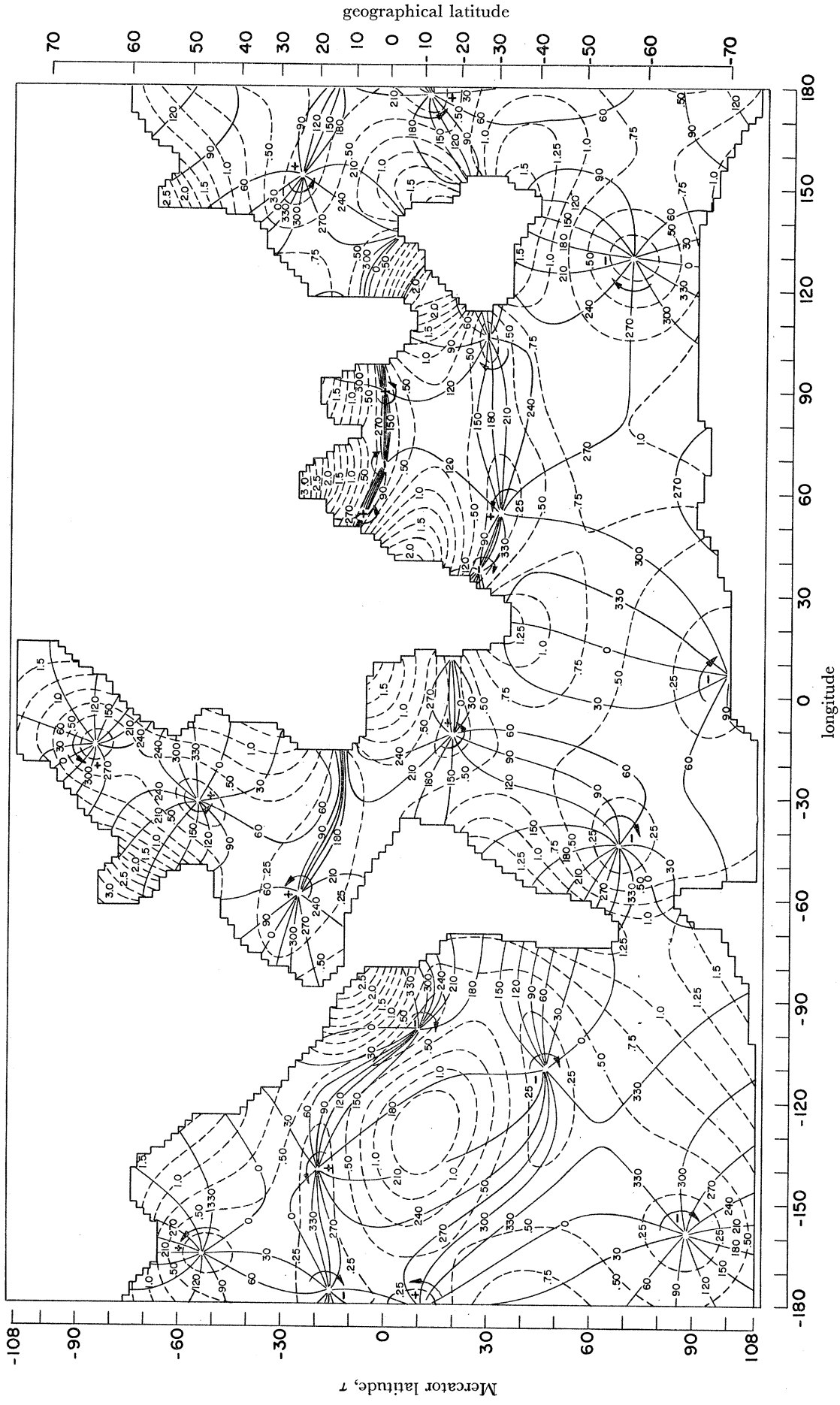

FIGURE 4. Cotidal lines (——) and corange lines (metres) (– – –) for the M_2 tide. Map 2° A; computation grid $k = 1°$; $f = \sigma/2\omega = 0.9635$.

PHILOSOPHICAL TRANSACTIONS OF THE ROYAL SOCIETY A MATHEMATICAL, PHYSICAL & ENGINEERING SCIENCES

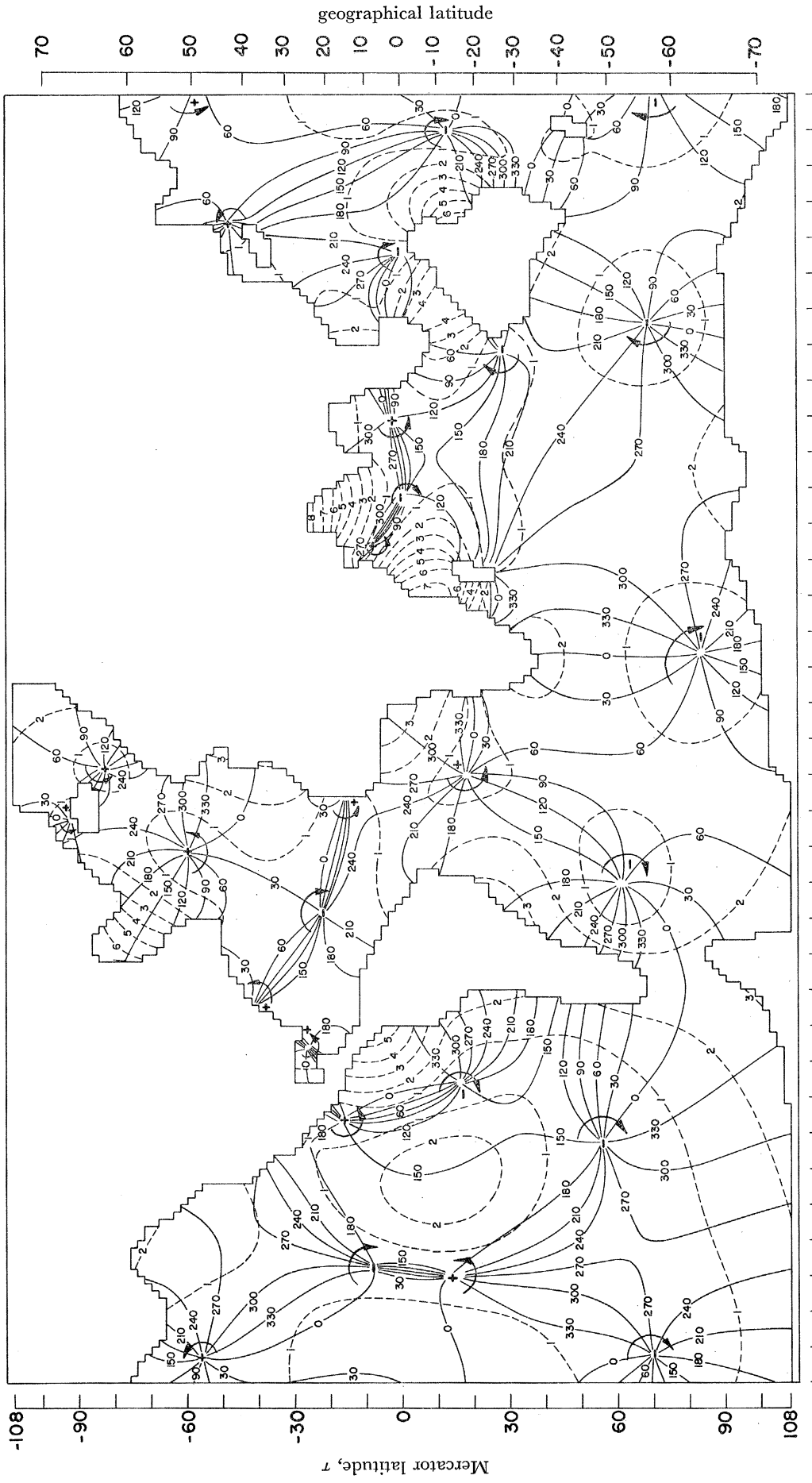

FIGURE 5. Cotidal lines (——) and corange lines (metres) (– – –) for the M_2 tide. Map 2° B; computation grid $k = 2°$; $f = \sigma/2\omega = 0.9635$

PHILOSOPHICAL TRANSACTIONS OF THE ROYAL SOCIETY A MATHEMATICAL, PHYSICAL & ENGINEERING SCIENCES

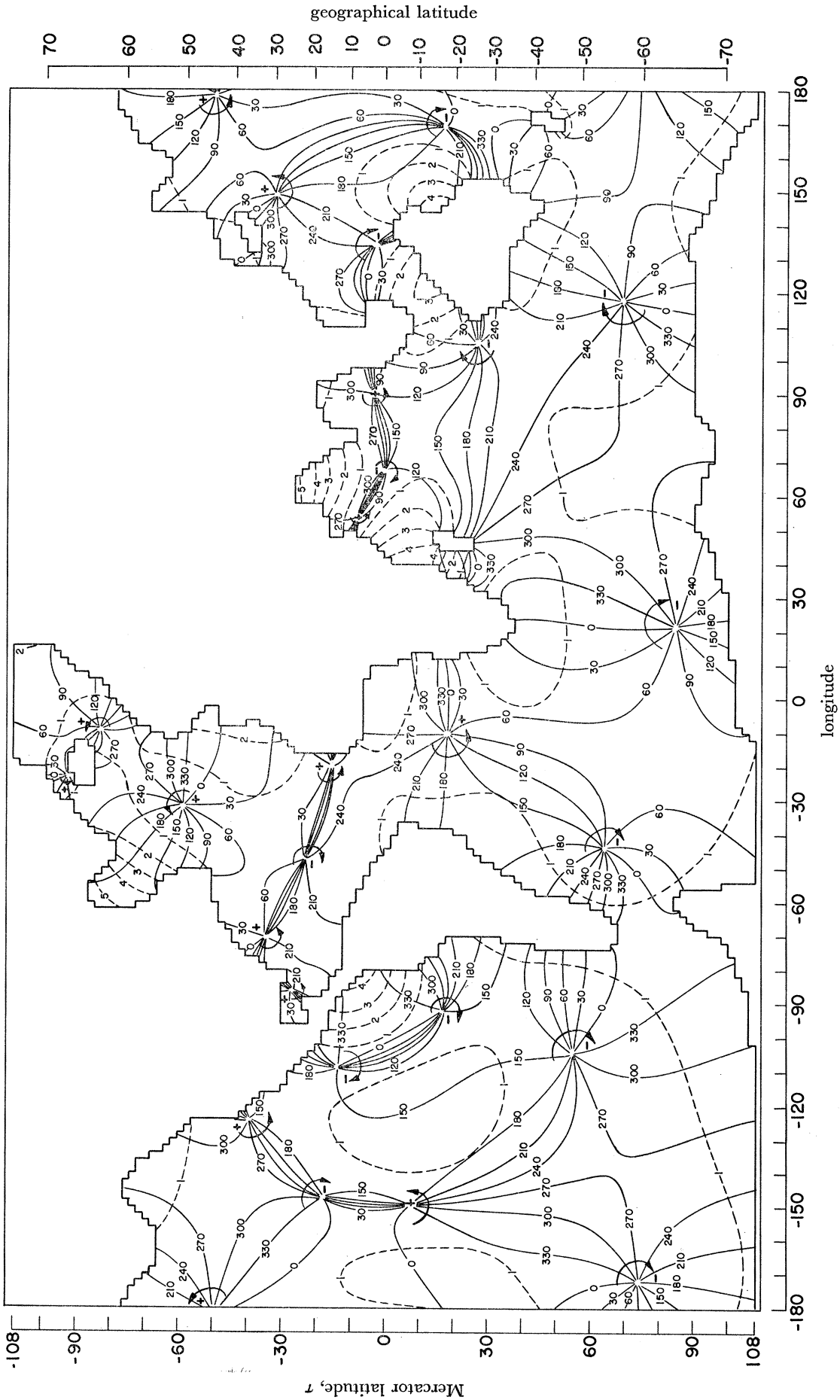

FIGURE 6. Cotidal lines (——) and corange lines (metres) (– – –) for the M_2 tide. Map 2° B; computation grid $k = 1°$; $f = \sigma/2\omega = 0.9635$.

PHILOSOPHICAL TRANSACTIONS OF THE ROYAL SOCIETY A MATHEMATICAL, PHYSICAL & ENGINEERING SCIENCES

publications of the International Hydrographic Bureau and the U.S. Navy Oceanographic Office (Dishon 1964). Where measurements were available, the depth at a grid point was taken as the average of the recorded depths inside the square of one degree.

These data were then subjected to a smoothing operation. The depth h at a given grid point was determined from the depths $h(d)$ in the neighbouring grid points, situated at a distance d from the station, through the smoothing operation (Dishon 1964)

$$h = \frac{\Sigma W(d)\, h(d)}{\Sigma W(d)}, \tag{1}$$

$$W(d) = (R^2 - d^2)/(R^2 + d^2). \tag{2}$$

We took the radius of smoothing R to be 12°. When a 5° radius R was tried, the numerical solution for the tides became unstable (in the case of the frictionless ocean model).

The total number of depth stations on which the map in figure 1 is based is 27 000. Over 1 million depth stations have now been processed (Dishon & Heezen 1968), from which a more representative topography of the ocean bottom will be obtainable.

(*b*) *Solution of Laplace's tidal equations for model oceans defined by arcs of* 2°, *and by arcs of* 1°

We have solved Laplace's tidal equations for the M_2 tide in the 1° ocean shown in figure 1, and the results are shown in figure 2. The dashed lines are *corange* lines, and the tidal amplitude is given in metres. The solid lines are *cotidal* lines referring to the time of Moon-transit through the meridian of Greenwich. With a tidal potential having a form $K\cos(\sigma t+\lambda)$, our tidal height has the form $A\cos(\sigma t+\psi)$. Hence the phases ψ written on the cotidal lines correspond to lunar hours for the time of high tide after lunar transit at Greenwich, as follows:

ψ	0	330	300	270	240	210	180	150	120	90	60	30
h	0	1	2	3	4	5	6	7	8	9	10	11.

One notes a number of *amphidromic systems* in which the amplitude of the tide vanishes. If we denote the *sense* of an amphidromic system as the direction in which high tide occurs progressively *later*, then generally the rotation of the tide in the amphidromic systems is in the direction of the Earth's rotation, i.e. counter-clockwise (cyclonic) in the Northern Hemisphere, and clockwise in the projection of the Southern Hemisphere. Most of our results refer to a '2° ocean', in which the coastline is defined by arcs of 2° in longitude and latitude.

Before discussing the actual solutions which we obtained, let us stop to reflect on the type of results we may expect. Were our tidal solution—based as it is on the assumption of complete neglect of friction—to yield tidal ranges and tidal phases which agree with tidal observations, then we should consider such a solution as unsatisfactory. Friction would be expected to reduce the ranges and to cause a delay in the times of high tide. The solutions which we obtained for a frictionless ocean do meet these criteria. Our tide ranges are never smaller than the observed tidal ranges, and our tidal phases show an advance of about 3 h relative to the observed tidal phases.

Consider the solution for the 2° ocean shown in figure 3. In this ocean there are about 12 000 grid points leading to a system of 46 400 real equations for the amplitudes and the phases of the two components of velocity. In the North Atlantic we find three amphidromic systems, one near the Faeroe Islands, another, the principal one, at about 48° N, 31° W, and a third one in the

PHILOSOPHICAL TRANSACTIONS OF THE ROYAL SOCIETY A MATHEMATICAL, PHYSICAL & ENGINEERING SCIENCES

TABLE 1. COMPARISON OF EMPIRICAL COORDINATES OF AMPHIDROMIC SYSTEMS (G. DIETRICH) WITH THEORETICAL ONES

(The signs denote the sense of the amphidromic systems. α denotes the coefficient of bottom friction defined in figure 10)

			G. Dietrich (Hansen 1952*a*)			map 2° *A*, *k* = 1° figure 4, $\alpha = 0$			map 2° *B*, *k* = 1° figure 6, $\alpha = 0$			map 2° *B*, *k* = 1° figure 9, $\alpha = 0.5$			map 1° *A*, *k* = 1° figure 2, $\alpha = 0$			map 1° *A*, *k* = 1° figure 10, $\alpha = 0.5$		
no.	location																			
1	Faeroe Islands	+	62° N	6° W	+	65° N	15° W	+	64° N	9° W	+	65° N	10° W	+	64° N	8° W	+	65° N	11° W
2	North Atlantic	+	52° N	33° W	+	48° N	31° W	+	51° N	31° W	+	50° N	36° W	+	51° N	33° W	+	50° N	38° W
3	Caribbean Sea	+	15° N	67° W	+	24° N	59° W	+	33° N	71° W	+	16° N	66° W	+	29° N	68° W	+	20° N	65° W
4	East South Atlantic	−	55° S	15° E	−	70 °S	7° E	−	64° S	22° E	−	65° S	30° E	−	56° S	23° E	−	64° S	36° E
5	East Central Pacific	−	2° S	103° W	−	10° S	98° W	−	16° S	92° W	−	14° S	96° W	−	15° S	96° W	−	14° S	95° W
6	East South Pacific	−	40° S	105° W	−	42° S	110° W	−	48° S	105° W	−	53° S	108° W	−	49° S	100° W	−	58° S	101° W
7	Middle South Pacific	−	51° S	160° W	−	66° S	158° W	−	59° S	172° W	−	50° S	157° W	−	47° S	160° W	−	49° S	160° W
8	West South Atlantic	K	.	.	−	56° S	44° W	−	54° S	44° W	−	60° S	47° W	−	47° S	34° W	−	62° S	57° W
9	East South Indian	−	33° S	103° E	−	58° S	130° E	−	57° S	117° E	−	29° S	107° E	−	58° S	99° E	−	33° S	105° E
10	West South Pacific	−	47° S	155° E	.	.	.	.	.	.	−	43° S	137° E	−	46° S	150° E	−	44° S	142° E
11	Middle Central Pacific	+	5° S	152° W	.	.	.	+	8° S	149° W	+	21° S	134° W	.	.	.	+	22° S	131° W
12	North East Pacific	+	40° N	148° W	.	.	.	−	18° N	147° W	−	21° N	150° W	−	12° N	147° W	−	23° N	153° W
13	Middle South Atlantic	.	.	.	.	.	.	.	.	.	+	19° S	13° W	.	.	.	+	21° S	15° W
14	North Indian	.	.	.	.	.	.	.	.	.	+	3° N	81° E	.	.	.	+	6° N	79° E
15	Arabian Sea	−	10° N	63° E	.	.	.	.	.	.	−	2° N	64° E	.	.	.	−	3° N	62° E

Caribbean Sea. The locations of these agree with those which have been deduced previously by Dietrich and predecessors from tidal observations on the coasts. The first question we want to ask is, how reliable is the solution? In this solution we used a computational grid k of 2° for an ocean whose coastline is defined by arc lengths of 2°.

In order to ascertain the degree of convergence of the 2° solution, we undertook to determine the tide in this ocean using a computational grid k of only 1°. The $k = 1°$ solution of map 2° A is shown in figure 4. There is hardly any change in amplitudes, phases, and in the configuration of the amphidromic systems as we go from the $k = 2°$ solution shown in figure 3 to the $k = 1°$ solution shown in figure 4.

Next, we take map 2° B, in which we introduced Iceland, New Zealand, Madagascar, Japan, and we have also refined the coastline by adding bays, etc. The $k = 2°$ solution of this model ocean, shown in figure 5, has a configuration of amphidromic systems which has changed little from map 2° A. However, the maximum tidal ranges have increased from 3 m to about 8 m. This would indicate a sensitivity of the tidal solution to details in the configuration of the coast. In order to ascertain the degree of convergence of the solution, we have again carried out a solution for this 2° B ocean using a computational grid of only $k = 1°$. The results are shown in figure 6. The maximum tidal range in the North Atlantic has been reduced from 6 m in figure 5 to 5 m in figure 6. In the Bay of Bengal, an initial tide of 8 m was reduced to 5 m.

The conclusion that suggests itself from these results, which were obtained for a *frictionless ocean*, is that (*a*) the tidal solution is sensitive to small changes in coastal configuration, and that (*b*) when the coast is 'rough', the computational grid-size k should be less than the grid of the coastline.

We now go back to the '1° ocean' shown in figure 2. Here the computational grid is $k = 1°$. The maximum tide height in the North Atlantic is now 12 m, while in the Bay of Bengal it is only 3 m. Still, the configuration of the amphidromic systems has not changed appreciably from maps 2° A and 2° B. This is shown in figure 7, which gives our three solutions for the North Atlantic, together with the semi-empirical solution derived by Hansen (1952*b*) from coastal observations. A noteworthy feature is the observed crowding of cotidal lines around Dakar, which all our three theoretical solutions reproduce. Also reproduced is the nearly horizontal belt of cotidal lines stretching from the Caribbean to Dakar. We also note that the cotidal lines of Hansen's map are about 3 h later than in our maps.

Table 1 gives the coordinates of the major amphidromic systems in our three solutions ($\alpha = 0$), together with those determined empirically by Dietrich (Hansen 1952*a*). The agreement is generally good.

3. Solution of Laplace's tidal equations under the assumption of a bottom friction force proportional to the velocity

(*a*) *Bottom friction*

Our solutions for a frictionless ocean, presented above, have given generally too large tidal amplitudes, and phases which are advanced by about three hours relative to the observed tides. They have also shown a sensitivity to changes in the configuration of the coast. All of these features would be expected to be improved by the introduction of friction. The magnitude of tidal friction can be estimated from the tidal dissipation which is required to account for the observed lunar secular acceleration. Munk & MacDonald (1960) arrive at a value of 2.7 TJ/s

for the astronomically determined lunar rate of tidal dissipation, while Jeffreys's estimate (Jeffreys 1962) is about half that value.

Now the generally accepted law of bottom friction for the ocean is represented by a frictional force per unit area $\boldsymbol{F}_B$ which is proportional to the square of the velocity $\boldsymbol{U}$

$$\boldsymbol{F}_B = -\kappa\rho\boldsymbol{U}|U|. \tag{3}$$

The drag coefficient κ is taken to have the value of 0.002. This value was found to hold for the drag of the wind on the ground, as well as for bottom friction in rivers and in tidal currents. Taylor (1919), in his investigation of tidal friction in the Irish Sea, found that the above value of κ applies there also.

Instead of the realistic square law of frictional force given in (3), we shall assume, in the first instance, a linear law

$$\boldsymbol{F}_B = -\rho r\boldsymbol{U}. \tag{4}$$

This approximation is made for analytical convenience, but is considered to be adequate for our immediate purpose, which is to study the general nature of the modification of our tidal solution caused by the introduction of frictional forces.

(*b*) *Laplace's tidal equations in the presence of bottom friction*

Now with the linear frictional law given in (4), Laplace's tidal equations become

$$\frac{\partial u}{\partial t} - 2\omega v\cos\theta = -\frac{g}{a}\frac{\partial\zeta'}{\partial\theta} - \frac{r}{h}u, \tag{5}$$

$$\frac{\partial v}{\partial t} + 2\omega u\cos\theta = -\frac{g}{a\sin\theta}\frac{\partial\zeta'}{\partial\lambda} - \frac{r}{h}v, \tag{6}$$

where u and v are the southern and eastern components of tidal velocity in a spherical system of coordinates,

$$h = h(\theta,\lambda) \tag{7}$$

is the measured ocean depth at colatitude θ and longitude λ,

$$\zeta' = \zeta - \bar{\zeta}, \quad \bar{\zeta} = -\Omega/g, \tag{8}$$

$\bar{\zeta}$ is the equilibrium tide, and Ω denotes the tidal potential. The variable depth $h(\theta, \lambda)$ also enters the equation of continuity,

$$\frac{\partial\zeta}{\partial t} = -\frac{1}{a\sin\theta}\left\{\frac{\partial}{\partial\theta}(hu\sin\theta) + \frac{\partial(hv)}{\partial\lambda}\right\}, \tag{9}$$

which serves to determine the tidal height ζ.

In order to avoid differentiating $h(\theta, \lambda)$ explicitly, we follow Love (1913) and make the substitution

$$hu = \frac{a}{\sin\theta}\frac{\partial F}{\partial t}, \quad hv = a\sin\theta\frac{\partial G}{\partial t}, \tag{10}$$

$$\zeta = -\frac{1}{\sin\theta}\frac{\partial F}{\partial\theta} - \frac{\partial G}{\partial\lambda} = \frac{\partial F}{\partial x} - \frac{\partial G}{\partial\lambda}, \quad x = \cos\theta, \tag{11}$$

whereby equation (9) reduces to (11), requiring no explicit differentiation of $h(\theta, \lambda)$. Equations (5) and (6) then yield

$$R[f^2(1-\mathrm{i}\gamma)F + \mathrm{i}f\sin^2\theta\cos\theta G] + h\sin\theta\frac{\partial}{\partial\theta}\left(\frac{1}{\sin\theta}\frac{\partial F}{\partial\theta} + \frac{\partial G}{\partial\lambda} + \bar{\zeta}\right) = 0, \tag{12}$$

PHILOSOPHICAL TRANSACTIONS OF THE ROYAL SOCIETY A MATHEMATICAL, PHYSICAL & ENGINEERING SCIENCES

$$R[f^2(1-\mathrm{i}\gamma)\sin^2\theta G - \mathrm{i}f\cos\theta F] + h\frac{\partial}{\partial\lambda}\left(\frac{1}{\sin\theta}\frac{\partial F}{\partial\theta} + \frac{\partial G}{\partial\lambda} + \bar{\zeta}\right) = 0, \tag{13}$$

$$f = \sigma/2\omega, \quad R = 4\omega^2 a^2/g = 88\,166 \text{ m}, \tag{14}$$

$$\gamma(\theta, \lambda) = r/\sigma h(\theta, \lambda). \tag{15}$$

Here a factor of $\mathrm{e}^{\mathrm{i}\sigma t}$ was assumed for all variables.

We now make the transition to the Mercator latitude τ

$$\tau = ln\tan\tfrac{1}{2}\theta, \quad \beta(\theta, \lambda) = R/h(\theta, \lambda), \tag{16}$$

and obtain

$$\beta f^2(1-\mathrm{i}\gamma)\, F - \mathrm{i}f\beta\frac{\sinh\tau}{\cosh^3\tau}G + \frac{\partial}{\partial\tau}(\cosh^2\tau F_\tau + G_\lambda + \bar{\zeta}) = 0, \tag{17}$$

$$\frac{\beta f^2(1-\mathrm{i}\gamma)}{\cosh^2\tau}G + \mathrm{i}\beta f\tanh\tau F + \cosh^2\tau F_{\tau\lambda} + G_{\lambda\lambda} = -\frac{2\mathrm{i}}{\cosh^2\tau}\mathrm{e}^{2\mathrm{i}\lambda}, \tag{18}$$

with

$$\bar{\zeta} = \sin^2\theta\,\mathrm{e}^{2\mathrm{i}\lambda} = \frac{1}{\cosh^2\tau}\mathrm{e}^{2\mathrm{i}\lambda}. \tag{19}$$

The unit of ζ is H''' which is equal to 24.25 cm for the M_2 tide. We have solved equations (17) and (18) by finite differences, imposing the boundary conditions of the vanishing of F along a coastal parallel, and of G along a meridianal segment of the coastline.

The effect of friction manifests itself only by the introduction of the factor $(1-\mathrm{i}\gamma)$ in equations (12), (13), (17) and (18). The depth $h(\theta, \lambda)$ appearing in the denominator in equation (15) for γ stems from the inertial mass of the whole column of water on which the frictional force at the bottom F_B acts.

(c) *The linear law of friction*

Now tidal friction is considered to be confined to the coastal areas and to be small in mid-ocean. In order to maximize tidal friction in shallow waters, we have put

$$\gamma = \frac{r}{\sigma h} = \alpha\left(\frac{h_0}{h}\right)^n, \tag{20}$$

where h_0 denotes the ocean depth near the coast, for which we have assumed a value of 1 km in our present calculations. The coefficient r in (4) therefore varies like $(h_0/h)^{n-1}$, giving greater emphasis to the coastal regions (for $n > 1$). In the tidal maps 8, 9 and 10, where friction was included, the value $n = 2$ was adopted.

As to the order of magnitude of the coefficient α in (20), we have some evidence from the investigation of Grace (1931) on tidal friction in the Gulf of Suez. Grace found that a value of $\alpha = 0.1$ fits the M_2 observations best. Interestingly, Grace applied both the linear friction law (4) and the quadratic law (3) and found that either one can account for the observed distribution of tidal amplitudes and phases in the Gulf of Suez ($h \simeq 44$ m), there being even a slight preference for the linear law.

Doodson (1956), in his study of tides and surges in a long uniform gulf, arrives at values of α for the diurnal (σ_1) tide ranging from 0.86 to 0.95. This would correspond to a value of α of about 0.5 for the M_2 tide (σ_2).

The above investigations indicate that where frictional effects are of importance, γ may reach a value as high as 0.5. These investigations were made for shallow waters of about 40 m depth only. Were we to scale down α to our assumed coastal depth h_0 of 1000 m, γ would be reduced to

PHILOSOPHICAL TRANSACTIONS OF THE ROYAL SOCIETY A MATHEMATICAL, PHYSICAL & ENGINEERING SCIENCES

about 0.02, and the frictional factor $(1-i\gamma)$ in equations (17) and (18) would then differ from unity by only 2 %. Accordingly, we set γ to have a value of from 0.1 to 0.5 *at the actual coast in our model ocean*, even though for the coastal depth assumed at present such frictional forces are excessive at the corresponding depth in the real oceans. As our ocean models become more refined in our future work and h_0 is reduced progressively, this formal discrepancy will be diminished. Another approach is to apply the tidal boundary conditions proposed by Jeffreys (1968) and Proudman (1941).

(*d*) *Tidal dissipation for a linear law of friction*

Under the assumption of the linear law of friction given in (4), the mean rate of dissipation of tidal energy per unit area per second is

$$\langle \boldsymbol{U}.\boldsymbol{F}_B\rangle = -\rho r\langle U^2\rangle. \tag{21}$$

If
$$U = A\cos(\sigma t+\psi), \tag{22}$$

then
$$\langle \boldsymbol{U}.\boldsymbol{F}_B\rangle = -\tfrac{1}{2}\rho r A^2 = -\tfrac{1}{2}\rho r(|u^2|+|v^2|), \tag{23}$$

where u and v are the meridional and longitudinal components of velocity given in (10). The total energy dissipated by tidal friction per second, D, is given by the integral of (23) over the oceanic areas:

$$D = \tfrac{1}{2}\rho a^2\iint \sin\theta\,\mathrm{d}\theta\,\mathrm{d}\lambda(|u^2|+|v^2|)r = \tfrac{1}{2}\rho a^4\sigma^2\iint \sin\theta\,\mathrm{d}\theta\,\mathrm{d}\lambda\left(\frac{F^2}{h^2\sin^2\theta}+\frac{\sin^2\theta}{h^2}G^2\right)r. \tag{24}$$

Substituting from equation (20) for r, and using the values

$$\rho = 1.026\ \mathrm{g/cm^3},\quad a = 6.371\times10^8\ \mathrm{cm},$$
$$h_0 = 10^5\ \mathrm{cm},\quad \sigma_2 = 1.401\times10^{-4}\ \mathrm{s^{-1}}, \tag{25}$$

we get
$$D_n = 2.33\times10^{18}\alpha\iint \sin\theta\,\mathrm{d}\theta\,\mathrm{d}\lambda(h_0/h)^{n+1}[(F^2/\sin^2\theta)+\sin^2\theta G^2]$$
$$= 2.33\times10^{18}\alpha\iint \mathrm{d}\tau\,\mathrm{d}\lambda(h_0/h)^{n+1}(F^2+\mathrm{sech}^4\tau G^2). \tag{26}$$

Here τ denotes the Mercator latitude defined in (16).

4. Discussion of results

In table 2 we have summarized the characteristic features of our solutions of Laplace's tidal equations, both for frictionless oceans ($\alpha = 0$) and for oceans with friction included. D_n denotes the mean rate of dissipation of energy by tidal friction, where n designates the assumed dependence of the frictional coefficient r in (4) on depth h, as defined in (20).

Map 2° *A* was designed to be smooth in that even Japan, New Zealand and Iceland were omitted, and the coastline was drawn so as to minimize sharp corners. It proved to be stable to the computational grid used (figures 3, 4), and the tidal heights came out reasonably moderate even without friction. On the other hand, map 2° *B* was drawn more realistically with no consideration given to smoothness. In the absence of friction (figure 5) and with a computational grid of $k = 2°$, the maximum tidal height reached an excessive value of 8.2 m, which was reduced to 5.3 m when the finer computational grid of $k = 1°$ was used (figure 6). When friction was introduced into this model and a value of $\alpha = 0.5$ was taken, with $n = 2$, the maximum tidal height was reduced to 3.3 m even for $k = 2°$, as shown in figure 8. This is of the

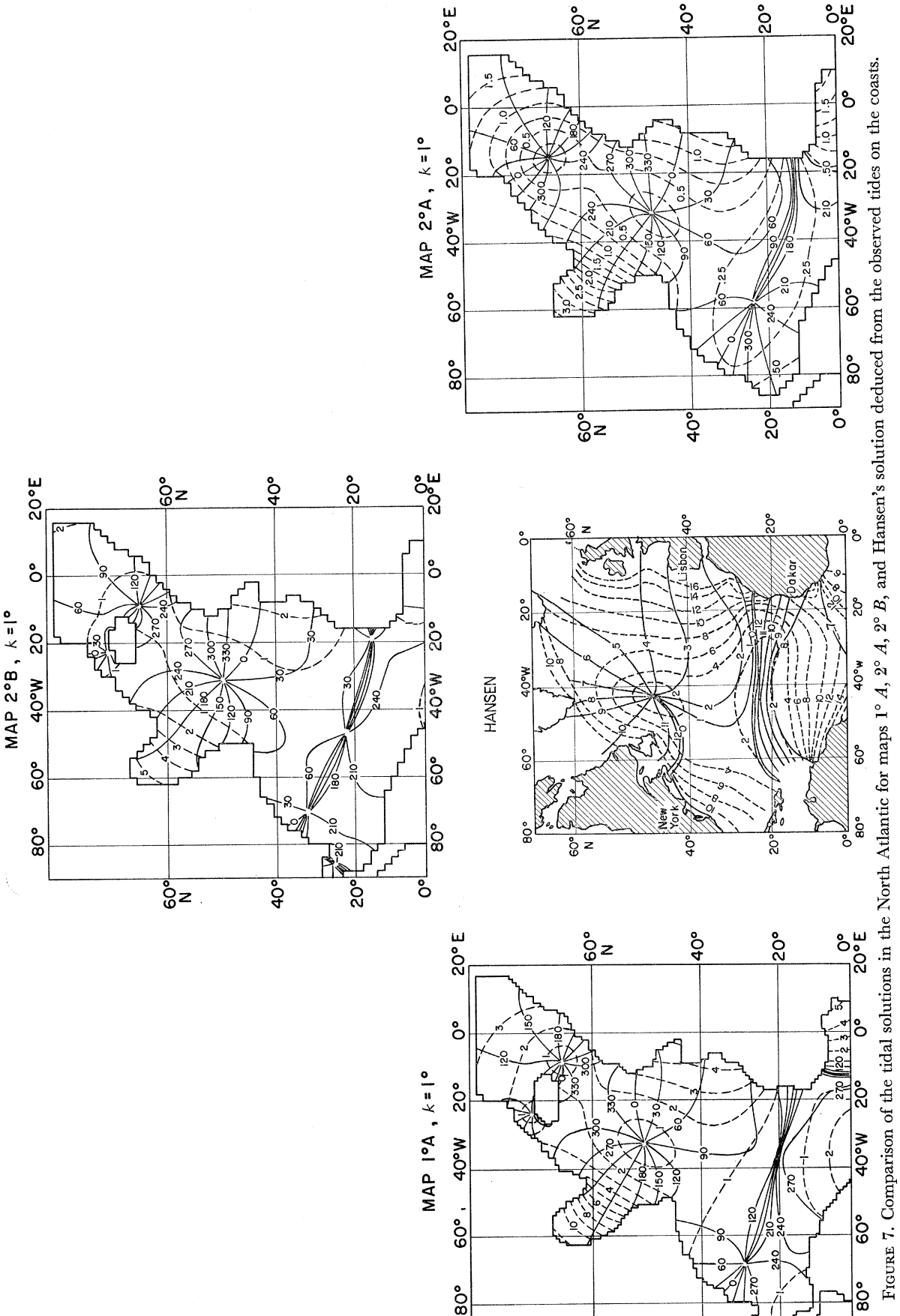

FIGURE 7. Comparison of the tidal solutions in the North Atlantic for maps 1° *A*, 2° *A*, 2° *B*, and Hansen's solution deduced from the observed tides on the coasts.

PHILOSOPHICAL TRANSACTIONS OF THE ROYAL SOCIETY A MATHEMATICAL, PHYSICAL & ENGINEERING SCIENCES

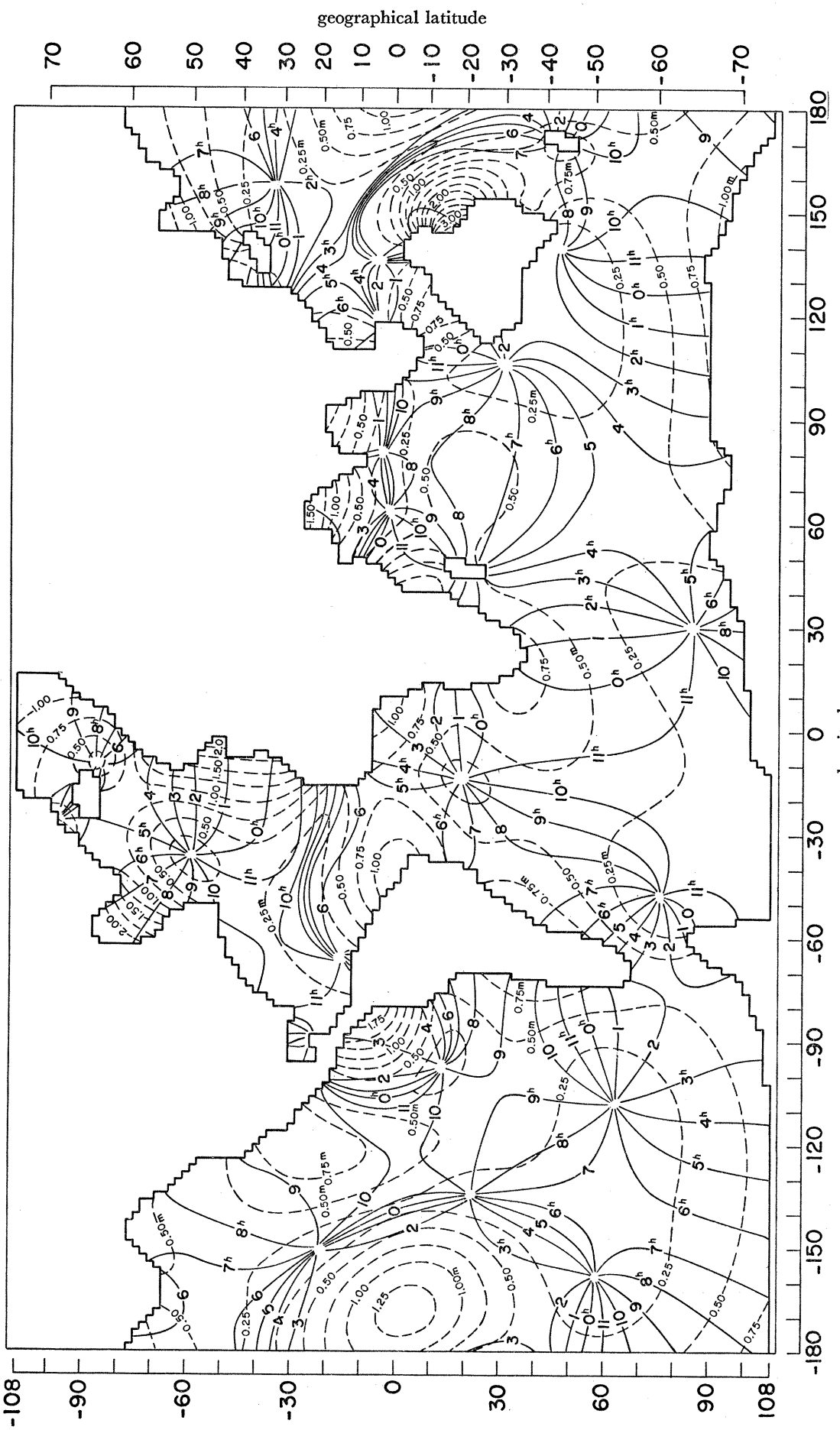

FIGURE 8. Cotidal lines (——) and corange lines (metres) (– – –) for the M_2 tide; map 2° B; computation grid, $k = 2°$; $f = \sigma_2/2\omega = 0.9635$; $F_B/\rho\sigma_2 h_0 = \alpha(h_0/h)^{n-1}U$ ($\alpha = 0.5$, $h_0 = 1$ km, $n = 2$, F_B = frictional force/unit area).

right magnitude observationally. We again proceeded to carry out a solution for this ocean model using a finer computational grid of $k = 1°$. The results are shown in figure 9. This shows that the solution in figure 8, with $k = 2°$, has already converged numerically.

TABLE 2. SOLUTION OF LAPLACE'S TIDAL EQUATIONS FOR THE M_2 TIDE IN A FRICTIONLESS OCEAN ($\alpha = 0$), AND WITH FRICTION INCLUDED ($\alpha \neq 0$).

The bottom friction is given by $\boldsymbol{F}_B = (\rho\sigma_2 h_0)\,\alpha(h_0/h)^{n-1}\boldsymbol{U}$. D_n denotes the mean rate of tidal dissipation by friction, $\boldsymbol{U}$ the velocity vector, and ζ the height of the tide. k denotes the computational grid used.

map	k	α	n	D_n / TJ/s	max$\lvert U\rvert$ / cm s^{-1}	max$\lvert\zeta\rvert$ / m	figure no.
1° *A*	1°	0	.	0	77	12.2	2
1° *A*	1°	0.5	2	6.6	21	3.4	10
2° *A*	2°	0	.	0	19	3.5	3
2° *A*	1°	0	.	0	21	3.3	4
2° *B*	2°	0	.	0	45	8.2	5
2° *B*	1°	0	.	0	35	5.3	6
2° *B*	2°	0.1	1	5.5	25	4.5	.
2° *B*	2°	0.1	2	4.5	28	6.5	.
2° *B*	2°	0.1	3	2.9	37	7.2	.
2° *B*	2°	0.2	3	4.6	31	6.8	.
2° *B*	2°	0.5	2	6.2	16	3.3	8
2° *B*	1°	0.5	2	6.0	18	3.2	9

Our theoretical value of around 6TJ/s for the rate of tidal dissipation by friction is higher than the values that have been deduced from the observed secular acceleration of the moon. Munk & MacDonald (1960) arrive at a value of 2.7 TJ/s for the lunar component of tidal dissipation, while Jeffreys's estimate is about half that value. With an uncertainty of a factor of 2 thus indicated in the observationally deduced value, it is premature to conclude that the tidal friction which we have introduced in our present calculations is excessive.

As to the phases of the tides, (figures 8, 9), when compared with figure 6, show that friction causes a retardation of tidal phases by about 1 h. On comparing the theoretical phases in the North Atlantic with Hansen's values based on observations shown in figure 7, it would seem that the retardation caused by friction is only about one-third of that required by the observations. Should this lack of agreement of the tidal phases persist in our future work, a clue might possibly be sought in the Earth tides.

Although the value of 0.5 assumed for the frictional parameter γ is high, it is to be noted that this value applies only to the coastline, and that away from the coastline γ falls off like $(h_0/h)^2$.

The results obtained so far with our preliminary solutions of Laplace's tidal equations indicate that friction may be an important controlling factor in the physics of ocean tides. It would be of interest to proceed with further refinement of the ocean models and with improvements in the assumed law of friction.

5. THE MIDDLE SOUTH ATLANTIC AMPHIDROME

On comparing figure 9 with figure 10, one notes that, when friction is included, the theoretical tidal charts for the two ocean models 1° *A* and 2° *B* come out very similar. This insensitivity to small changes in the coastal configuration is reflected also in the closeness of the positions of the amphidrome systems for figures 9 and 10, as shown in table 1.

The above results encourage the hope that figure 10 may already be a close approximation to the theoretical solution for the M_2 tide in the real world oceans. As a first test we took up a query by D. E. Cartwright of the National Institute of Oceanography as to the reality of the Middle South Atlantic amphidrome shown in figure 10. This amphidrome has not appeared previously in any of the empirically derived charts for the Atlantic Ocean (G. Dietrich, quoted by Hansen (1952*a*)). We have plotted this theoretical amphidrome, taken from figure 10, on the real ocean map shown in figure 11. We have also entered in figure 11 the observed phase-lags for the M_2 tide at several neighbouring island stations. With $\kappa°$ denoting the observed phase-lag of high tide behind local lunar transit, the corresponding lag behind lunar transit of Greenwich is given by $t_{\text{obs}} = (\kappa° + 2\lambda)/30$, in units of lunar hours. Here $\lambda°$ denotes the West longitude of the station. Values of t_{obs} are shown in figure 11 by the underlined numbers, while the amplitudes of the observed tides are given in parentheses. We note that the observed tidal retardation at each of the four neighbouring islands is within 1.2 h of the theoretical values. To the extent that these data are representative, they provide observational support for a tidal wave advancing in a counterclockwise direction around the amphidromic point situated at about 21° S, 15° W.

The observed retardations at the island of Fernando de Naronha, and at Elsehul in South Georgia, are also in good agreement with our theoretical values. However, at Stanley Harbour in the Falkland Islands the observed retardation is nearly 3 h greater than the theoretical value. This station is influenced by the neighbouring amphidrome to the south, whose position is seen to vary from figure 9 to figure 10. Similar variability in the positions of amphidromic centres is found in other shallow basins and straits, which could be approximated only roughly in our ocean model, such as the Caribbean Sea, Indonesia, the Eastern Pacific, and the Bering Sea.

Although the general appearance of our tidal charts in the Pacific are similar in figures 9 and 10, there is considerable variation for individual stations. The agreement of the theoretical tidal values with island observations is poor in the Northern Pacific; in particular, on the American Northwest coast the tide is observed to move northwards, as against a southerly tide given by our theoretical solution.

On the other hand, in the Atlantic and Indian Oceans the agreement at island stations with our theoretical tidal values is good, as seen in figure 11, and in table 3. For the island stations in the Atlantic and Indian oceans, the retardation t_{obs} exceeds t_{th} by only 1.2 h on the average, while the average value of $H_{\text{th}}/H_{\text{obs}}$ is 1.3.

6. The tidal velocity field for the M_2 tide

The tidal chart in figure 10, which was derived entirely from a solution of Laplace's tidal equations (5), (6) and (9) for the 1° *A* model of the world oceans shown in figure 1, gives the distribution of tidal amplitudes and phases. The corresponding tidal velocity field is shown in figure 12. This chart should be considered as of a preliminary nature only. It is presented here in response to requests by many geophysicists engaged in different fields of application, including the direct measurement of tidal currents in the deep sea.

Now the tidal velocity field can be readily derived, since in our method the velocity functions F and G are obtained directly from the solution of equations (17) and (18). The components of velocity u and v are then given by equation (10).

PHILOSOPHICAL TRANSACTIONS OF THE ROYAL SOCIETY A MATHEMATICAL, PHYSICAL & ENGINEERING SCIENCES

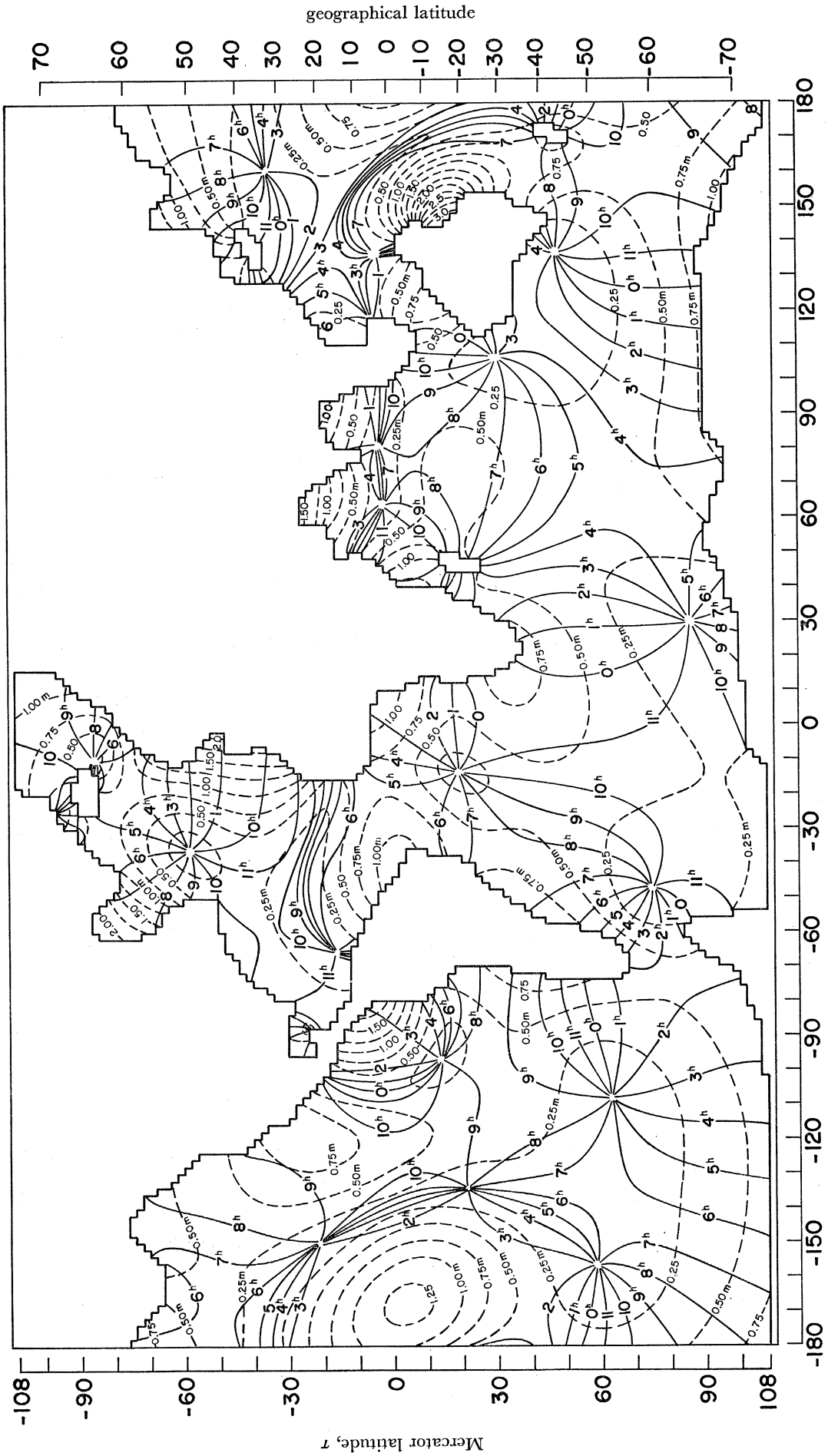

FIGURE 9. Cotidal lines (——) and corange lines (metres) (– – –) for the M_2 tide; map 2° B; computation grid $k = 1°$; $f = \sigma_2/2\omega = 0.9635$; $\boldsymbol{F}_B/\rho\sigma_2 h_0 = \alpha(h_0/h)^{n-1}\boldsymbol{U}$ ($\alpha = 0.5$, $h_0 = 1$ km, $n = 2$, $\boldsymbol{F}_B$ = frictional force/unit area).

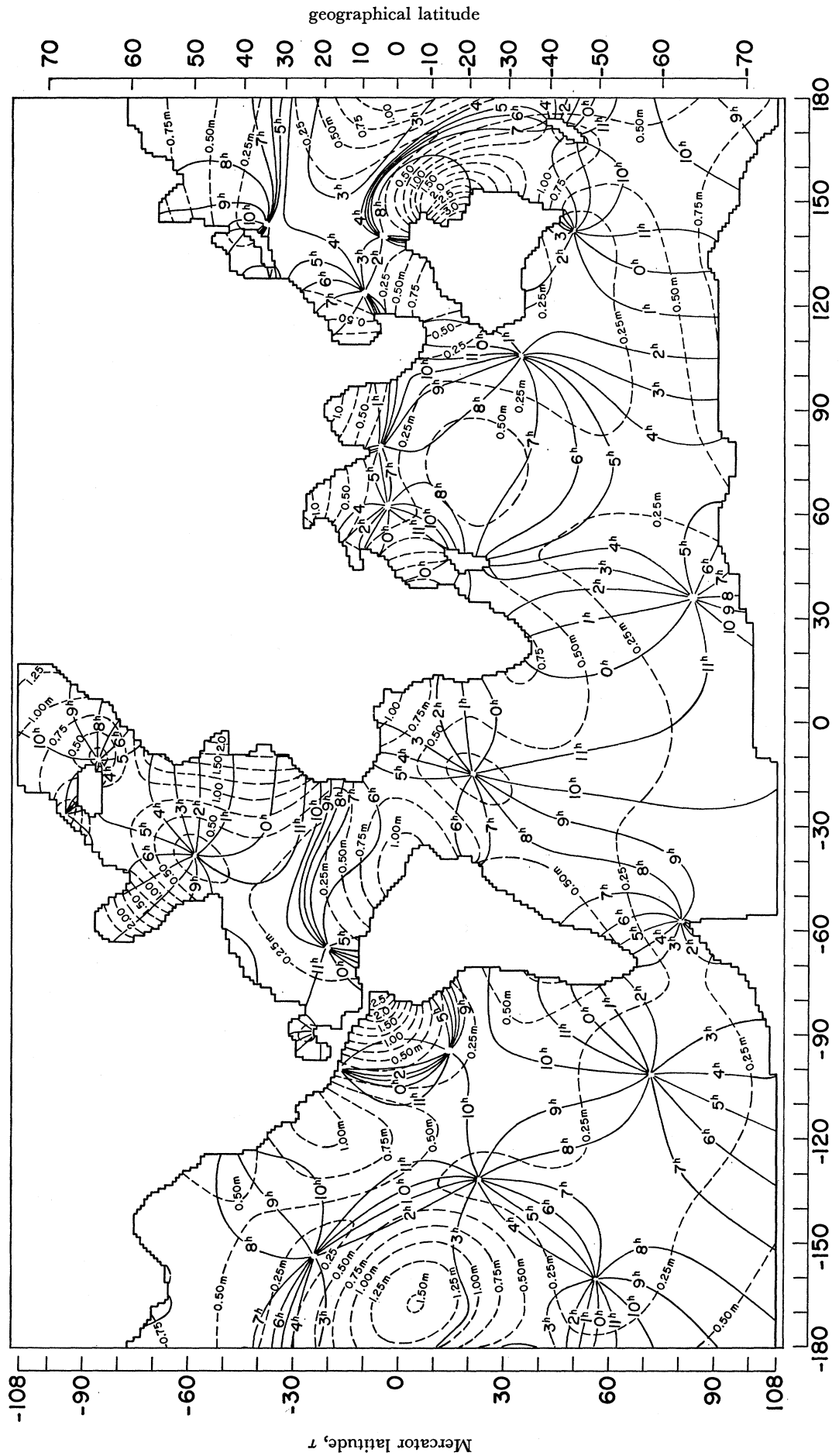

FIGURE 10. Cotidal lines (——) and corange lines (metres) (– – –) for the M_2 tide; map 1° A; computation grid, $k = 1°$; $f = \sigma_2/2\omega = 0.9635$; $F_B/\rho\sigma_2 h_0 = \alpha(h_0/h)^{n-1}U$ ($\alpha = 0.5$, $h_0 = 1$ km, $n = 2$, F_B = frictional force/unit area).

In representing the velocity field, we must of course recognize that u and v have different phases:

$$u = A\cos(\sigma t + \psi), \tag{27}$$

$$v = B\cos(\sigma t + \phi), \tag{28}$$

TABLE 3. COMPARISON OF TIDAL OBSERVATIONS ON ISLANDS WITH THEORETICAL VALUES

(H is the amplitude of the M_2 tide, and t denotes the phase lag)

station	area	I.H.B. reference	latitude	longitude	H_{obs} cm	H_{th} cm	t_{obs} h	t_{th} h
North Atlantic Ocean								
Flores I.	Azores	2204	39° 23′ N	31° 11′ W	39	60	2.0	0.4
Santa Maria I.	Azores	2203	36° 57′ N	25° 09′ W	51	85	2.0	0.3
Funchal	Madeira	377	32° 38′ N	16° 54′ W	72	130	1.5	11.9
Tenerife	Canary I.	2317	28° 29′ N	16° 14′ W	69	130	1.0	11.5
Santo Antao	Cape Verde I.	2204	17° 01′ N	25° 04′ W	30	40	8.7	8.0
Eleuthera I.	Bahama I.	2212	24° 56′ N	76° 09′ W	32	30	0.7	10.9
St George's I.	Bermuda	2170	32° 24′ N	64° 42′ W	37	30	0.0	10.5
South Atlantic Ocean								
Ascension I.	.	2257	7° 55′ S	14° 25′ W	51	45	5.8	4.6
Fernando de Noronha	.	1040	3° 50′ S	32° 24′ W	79	100	6.9	5.8
St Helena I.	.	ATT′ 38	15° 55′ S	5° 42′ W	34	45	2.9	1.7
Isla Trinidade	.	ATT′ 69	20° 30′ S	29° 20′ W	34	45	7.0	6.5
Tristan da Cunha	.	ATT′ 38	37° 02′ S	12° 18′ W	34	40	11.8	10.8
Stanley Harbour	Falkland I.	2321	51° 42′ S	57° 51′ W	45	45	9.1	6.3
Elsehul	South Georgia	1101	54° 02′ S	38° 00′ W	27	25	9.0	8.3
Scotia Bay	South Orkney I.	2321	60° 44′ S	44° 39′ W	46	15	8.7	8.3
Indian Ocean								
Port Victoria	Seychelles I.	2137	4° 37′ S	55° 27′ E	40	35	0.4	11.1
Port Louis	Mauritius	24	20° 09′ S	57° 29′ E	13	50	8.9	7.5
Addu Atoll	.	1099	0° 34′ S	73° 13′ E	29	25	8.4	7.5
Port Refuge	Cocos I.	2208	12° 05′ S	96° 53′ E	27	25	10.4	9.0
St Paul I.	.	2196	38° 43′ S	77° 35′ E	38	40	7.7	6.7
Port-aux-Francais	Kerguelen	2348	49° 21′ S	70° 13′ E	51	30	6.5	5.3
North Pacific Ocean								
Pagan I.	Marianas I.	3048	18° 08′ N	145° 46′ E	17	10	9.8	3.5
Kusaie I.	Caroline I.	3049	5° 20′ N	163° 01′ E	42	30	4.3	2.9
Port Rhin	Marshall I.	3048	6° 14′ N	171° 48′ E	57	80	4.4	2.8
Midway I.	.	2210	28° 12′ N	177° 22′ W	11	25	3.0	4.0
Johnston I.	.	2167	16° 45′ N	169° 30′ W	27	80	3.5	2.9
Honolulu	Hawaiian I.	649	21° 18′ N	157° 52′ W	16	25	2.1	3.2
South Pacific Ocean								
Lord Howe I.	Tasman Sea	940	31° 32′ S	159° 04′ E	59	135	10.1	7.5
Paagoumene Bay	New Caledonia	2147	20° 29′ S	164° 11′ E	45	110	9.0	7.5
Vila Harbour	New Hebrides	1095	17° 45′ S	168° 19′ E	34	60	6.9	7.1
Kingston	Norfolk I.	2232	29° 04′ S	167° 56′ E	57	75	8.8	7.1
Nukualofa	Tonga I.	1092	21° 08′ S	175° 13′ W	52	85	6.4	3.3
Funafuti	Ellice I.	2172	8° 32′ S	179° 12′ E	57	100	5.1	2.9
Aitutaki	Cook I.	2233	18° 51′ S	159° 47′ W	17	110	7.0	3.1
Hanga Piko	Easter I.	948	27° 09′ S	109° 27′ W	21	35	0.5	9.5
Caleta Aeolian	Galapagos I.	2168	0° 26′ S	90° 17′ W	72	100	8.2	5.9
Gambier I.	Polynesian Arch.	2348	23° 07′ S	134° 58′ W	27	15	11.6	4.0
Ahe	Polynesian Arch.	2347	14° 32′ S	146° 21′ W	12	80	2.9	2.9
Nukuhiva	Polynesian Arch.	2260	8° 55′ S	140° 06′ W	47	50	1.2	2.0

PHILOSOPHICAL TRANSACTIONS OF THE ROYAL SOCIETY A MATHEMATICAL, PHYSICAL & ENGINEERING SCIENCES

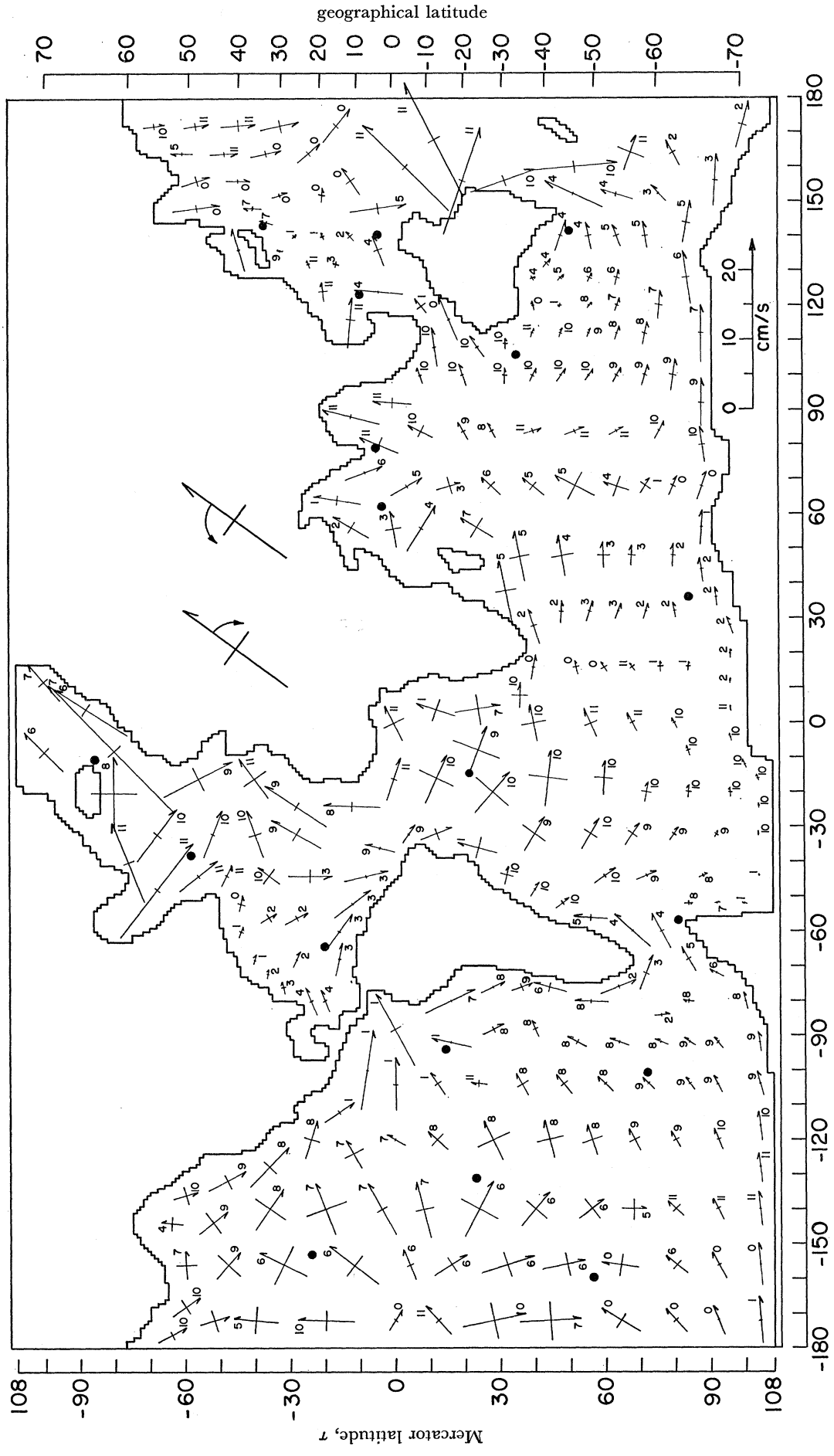

FIGURE 12. The velocity field for the M_2 tide shown in figure 10. Vectors give the major and minor axes of the velocity ellipse at the position of the centre. The arrow points in the direction of advance of the tide, as shown in the insert. The black circles designate positions of amphidromic centres.

PHILOSOPHICAL TRANSACTIONS OF THE ROYAL SOCIETY A MATHEMATICAL, PHYSICAL & ENGINEERING SCIENCES

so that the velocity vector traces out an ellipse during a tidal period, rather than a straight line. In figure 12 are shown the major and minor axes of the velocity ellipse at the position of centre. The velocity vector is the distance from the centre to the ellipse.

From (27) and (28) we get for the square of the velocity vector U^2

$$U^2 = u^2+v^2 = \tfrac{1}{2}(A^2+B^2)+\tfrac{1}{2}[A^4+B^4+2A^2B^2\cos(2\psi-2\phi)]^{\frac{1}{2}}\cos(2\sigma t-2\gamma), \tag{29}$$

$$\cos 2\gamma = \frac{(A^2\cos 2\psi+B^2\cos 2\phi)}{[A^4+B^4+2A^2B^2\cos(2\psi-2\phi)]^{\frac{1}{2}}}, \quad \sin 2\gamma = -\frac{(A^2\sin 2\psi+B^2\sin 2\phi)}{[A^4+B^4+2A^2B^2\cos(2\psi-2\phi)]^{\frac{1}{2}}}. \tag{30}$$

$$U^2_{\max} = \tfrac{1}{2}(A^2+B^2)+[A^4+B^4+2A^2B^2\cos(2\psi-2\phi)]^{\frac{1}{2}}, \tag{31}$$

$$U^2_{\min} = \tfrac{1}{2}(A^2+B^2)-\tfrac{1}{2}[A^4+B^4+2A^2B^2\cos(2\psi-2\phi)]^{\frac{1}{2}}. \tag{32}$$

Since the equilibrium tide $\bar{\zeta}$ appearing as the forcing function in the tidal equations was assumed, in (19), to have the form

$$\bar{\zeta} = K\cos(\sigma t+2\lambda), \tag{33}$$

it follows that our time-origin is lunar transit at the Greenwich meridian. Hence the times of maximum and minimum velocities are given by (29)

$$t_{\max} = \frac{\gamma}{\sigma} = \left(12+\frac{\gamma^\circ}{30}\right)\text{hours}, \tag{34}$$

$$t_{\min} = \frac{\gamma}{\sigma}\pm\frac{\pi}{2\sigma} = \left(12+\frac{\gamma^\circ}{30}\pm 3\right)\text{hours}. \tag{35}$$

We have indicated by circles on figure 12 the positions of the amphidromic centres. It is seen that, while the tide elevation vanishes at an amphidromic centre, the tidal current does not vanish, but maintains a value not noticeably different from its surroundings. One should therefore be able to measure tidal currents also in the vicinity of amphidromic centres.

This research was supported by the Office of Naval Research under contract N 00014–66–C0080 and by the National Science Foundation under Grant GA–1062. The reproduction of figure 11 has been facilitated by the Office of Naval Research, Washington, D.C., U.S.A., who kindly provided the negatives from which the printing plates were made.

References

Dishon, M. 1964 *Int. hydrogr. Rev.* **41**, 77.
Dishon, M. & Heezen, B. C. 1968 *Int. hydrogr. Rev.* **45**, 23.
Doodson, A. T. 1956 *Proc. Roy. Soc. Lond.* A **237**, 339.
Grace, S. F. 1931 *Mon. Not. R. astr. Soc. geophys. Suppl.* **2**, 316.
Hansen, W. 1952*a* *Landolt-Börnstein Handbuch*, Band III, p. 521. Berlin: Springer-Verlag.
Hansen, W. 1952*b* *Dt. hydrogy. Z.* Heft 1. Taken from G. Dietrich, *General oceanography*, p. 456. New York: Interscience Publishers, 1963.
Jeffreys, H. 1962 *The Earth* (4th ed.), p. 244. Cambridge University Press.
Jeffreys, H. 1968 *Geophys. J. R. astr. Soc.* **16**, 253.
Love, A. E. H. 1913 *Proc. Fifth. Int. Congr. Math.*, vol. II, p. 202. Cambridge University Press.
Munk, W. & MacDonald, G. J. F. 1960 *The rotation of the Earth: a geophysical discussion*, p. 217. Cambridge University Press.
Proudman, J. 1941 *Mon. Not. R. astr. Soc. geophys. Suppl.* **5**, 23.
Taylor, G. I. 1919 *Phil. Trans. Roy. Soc. Lond.* A **220**, 1.

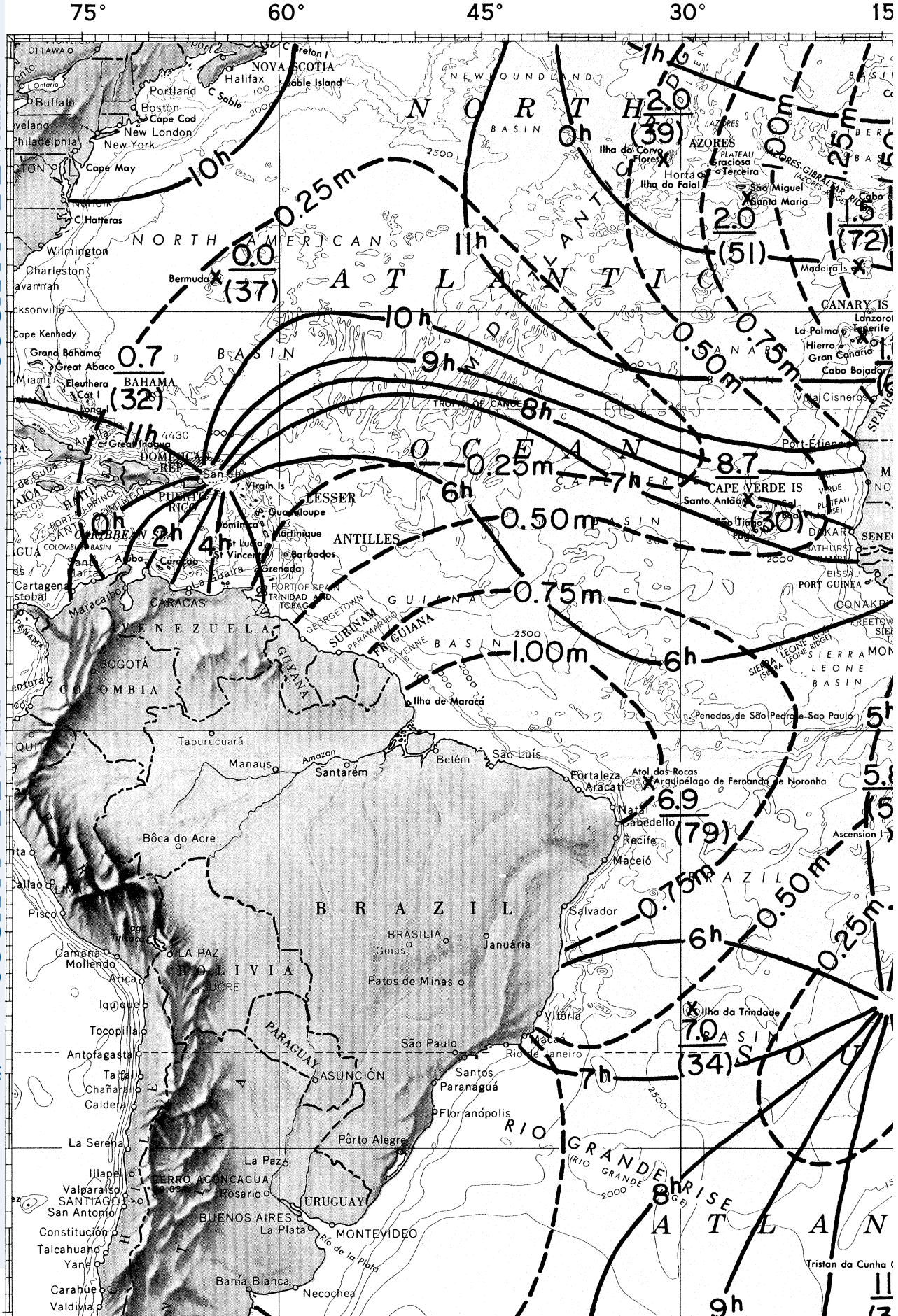

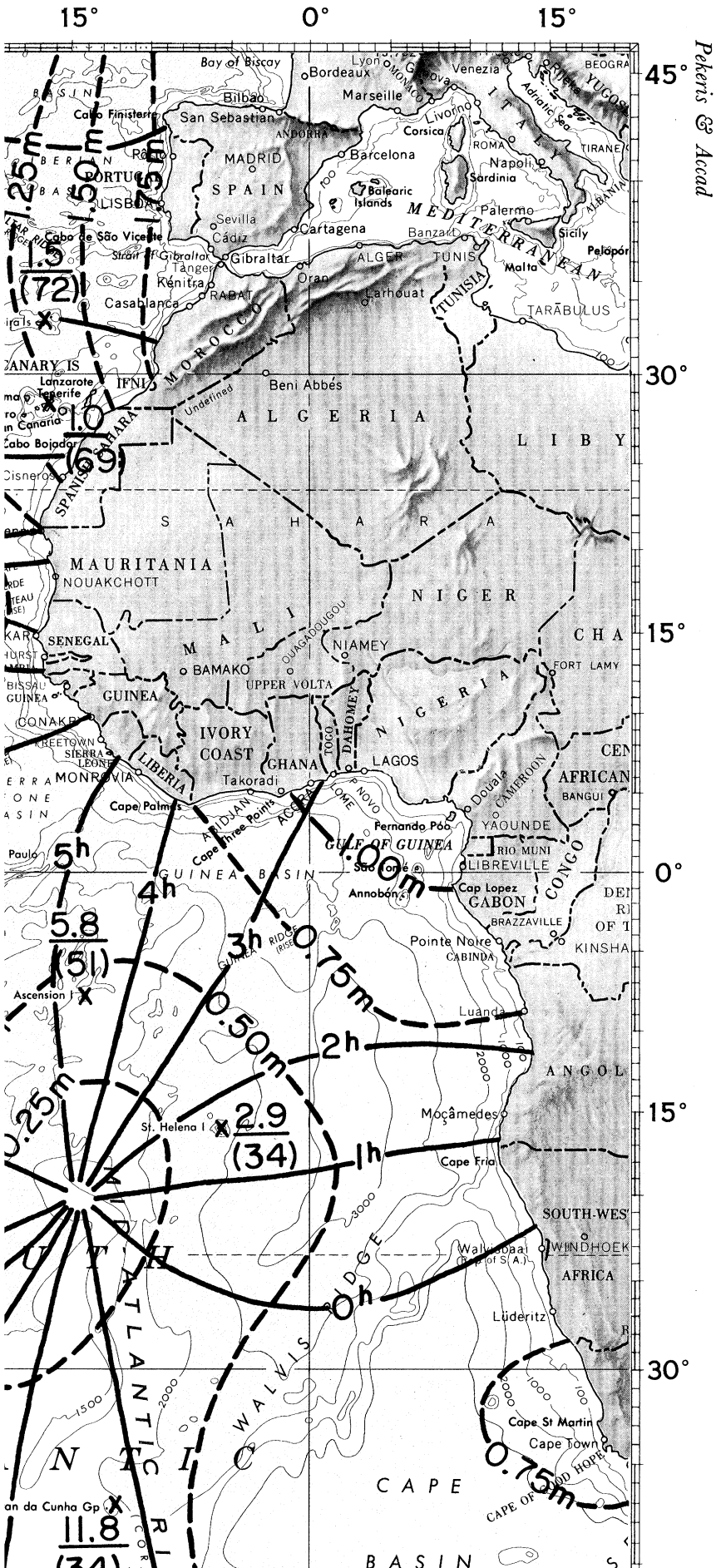
15°
0°
15°
45°
30°
15°
0°
15°
30°
Bay of Biscay
Bordeaux
Lyon
Marseille
Genova
Venezia
BEOGRA
YUGOS
Bilbao
Cabo Finisterre
San Sebastian
ANDORRA
Corsica
Livorno
ITALY
Adriatic Sea
ROMA
TIRANE
MADRID
Barcelona
Napoli
Sardinia
SPAIN
PORTUGAL
LISBON
Balearic Islands
MEDITERRANEAN
ALBANIA
Sevilla
Cartagena
Palermo
Cádiz
Cabo de São Vicente
Strait of Gibraltar
Gibraltar
Tánger
ALGER
TUNIS
Banzart
Sicily
Peloponn
Malta
Kénitra
RABAT
Oran
Casablanca
Larhouat
TUNISIA
TARĀBULUS
MOROCCO
CANARY IS
Lanzarote
Tenerife
Canaria
IFNI
Undefined
Beni Abbés
ALGERIA
LIBY
Cabo Bojador
SPANISH SAHARA
Cisneros
SAHARA
MAURITANIA
NOUAKCHOTT
NIGER
MALI
SENEGAL
BAMAKO
OUAGADOUGOU
NIAMEY
CHA
FORT LAMY
BISSAU
GUINEA
UPPER VOLTA
NIGERIA
CONAKRY
FREETOWN
SIERRA LEONE
IVORY COAST
GHANA
TOGO
DAHOMEY
LAGOS
LIBERIA
MONROVIA
Takoradi
CEN
AFRICAN
Douala
CAMEROON
BANGUI
Cape Palmas
ABIDJAN
ACCRA
Cape Three Points
Pernando Póo
YAOUNDE
GULF OF GUINEA
RIO MUNI
LIBREVILLE
São Tomé
Annobón
Cap Lopez
GABON
CONGO
DEI
R
OF T
BRAZZAVILLE
KINSHA
Pointe Noire
CABINDA
GUINEA BASIN
Luanda
ANGOL
Moçâmedes
St. Helena I
Cape Fria
SOUTH-WES
WINDHOEK
AFRICA
Walvisbaai
(Rep of S.A.)
Lüderitz
WALVIS RIDGE
Cape St Martin
Cape Town
CAPE OF GOOD HOPE
CAPE
BASIN
Ascension I
an da Cunha Gp
1.25m
1.5
(72)
1.0
(69)
5h
4h
3h
2h
1h
0h
1.00m
0.75m
0.50m
0.25m
5.8
(51)
2.9
(34)
11.8
(34)

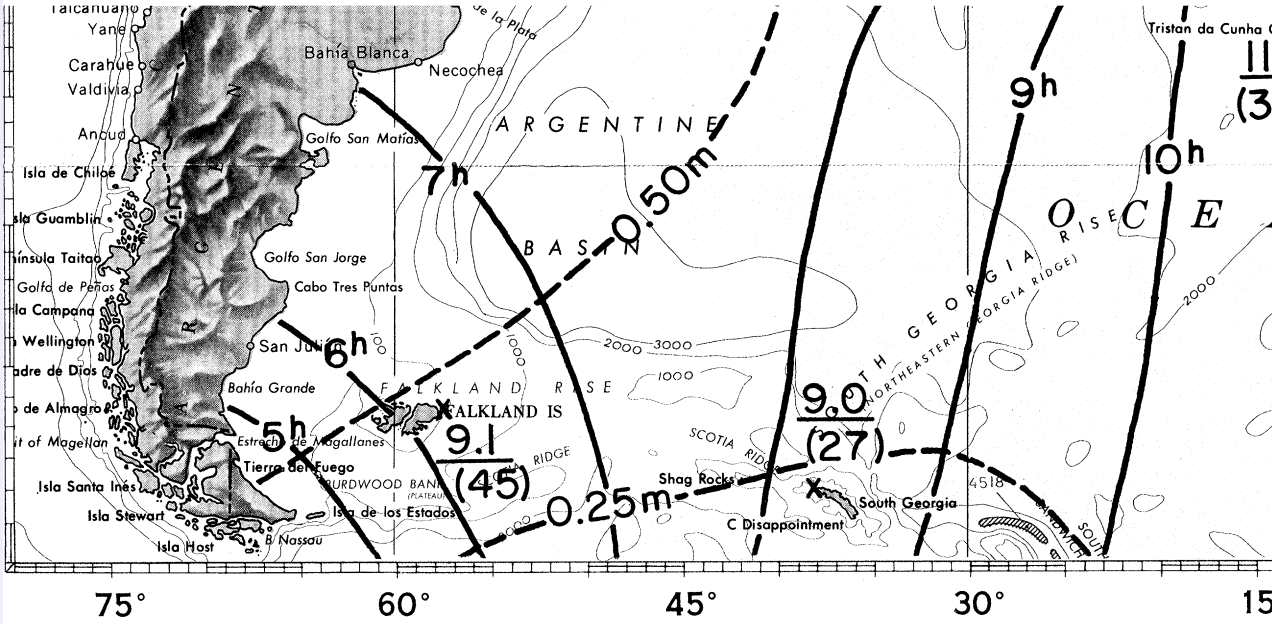

FIGURE 11. The Middle South Atlantic amphidrome (21 S, 15 W) for the M_2 ti
Underlined numbers give observed phase lags (in hours) of high tide, relative to th
Greenwich. Numbers in parentheses give the observed amplitudes in centimetres
lines; – – –, corange lines (in metres).

PHILOSOPHICAL TRANSACTIONS OF THE ROYAL SOCIETY A MATHEMATICAL, PHYSICAL & ENGINEERING SCIENCES

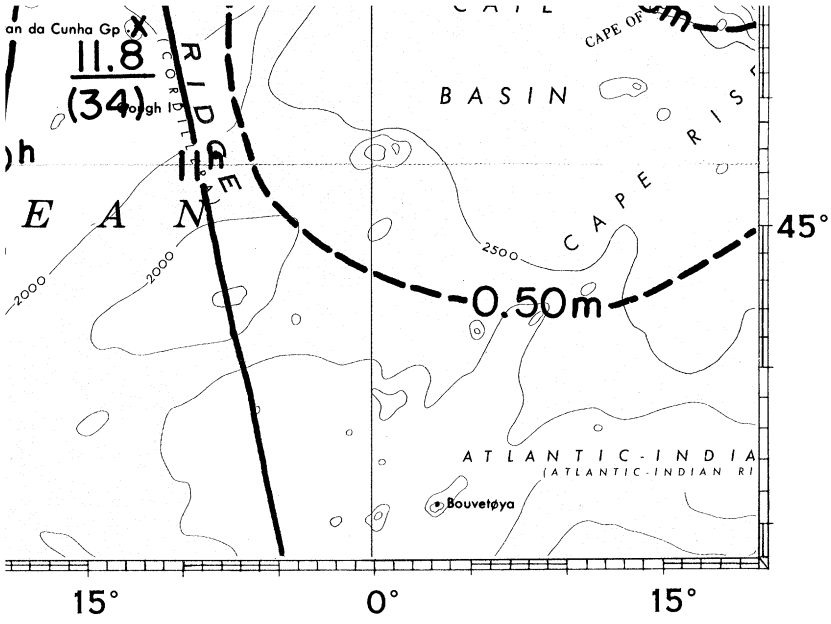

the M_2 tide, taken from figure 10.
ative to the time of lunar transit at
entimetres. ——, Theoretical cotidal

PHILOSOPHICAL TRANSACTIONS OF THE ROYAL SOCIETY A MATHEMATICAL, PHYSICAL & ENGINEERING SCIENCES

FIGURE 11. The Middle South Atlantic amphidrome (21 S, 15 W) for the M_2 tide, taken from figure 10. Underlined numbers give observed phase lags (in hours) of high tide, relative to the time of lunar transit at Greenwich. Numbers in parentheses give the observed amplitudes in centimetres. ——, Theoretical cotidal lines; – – –, corange lines (in metres).

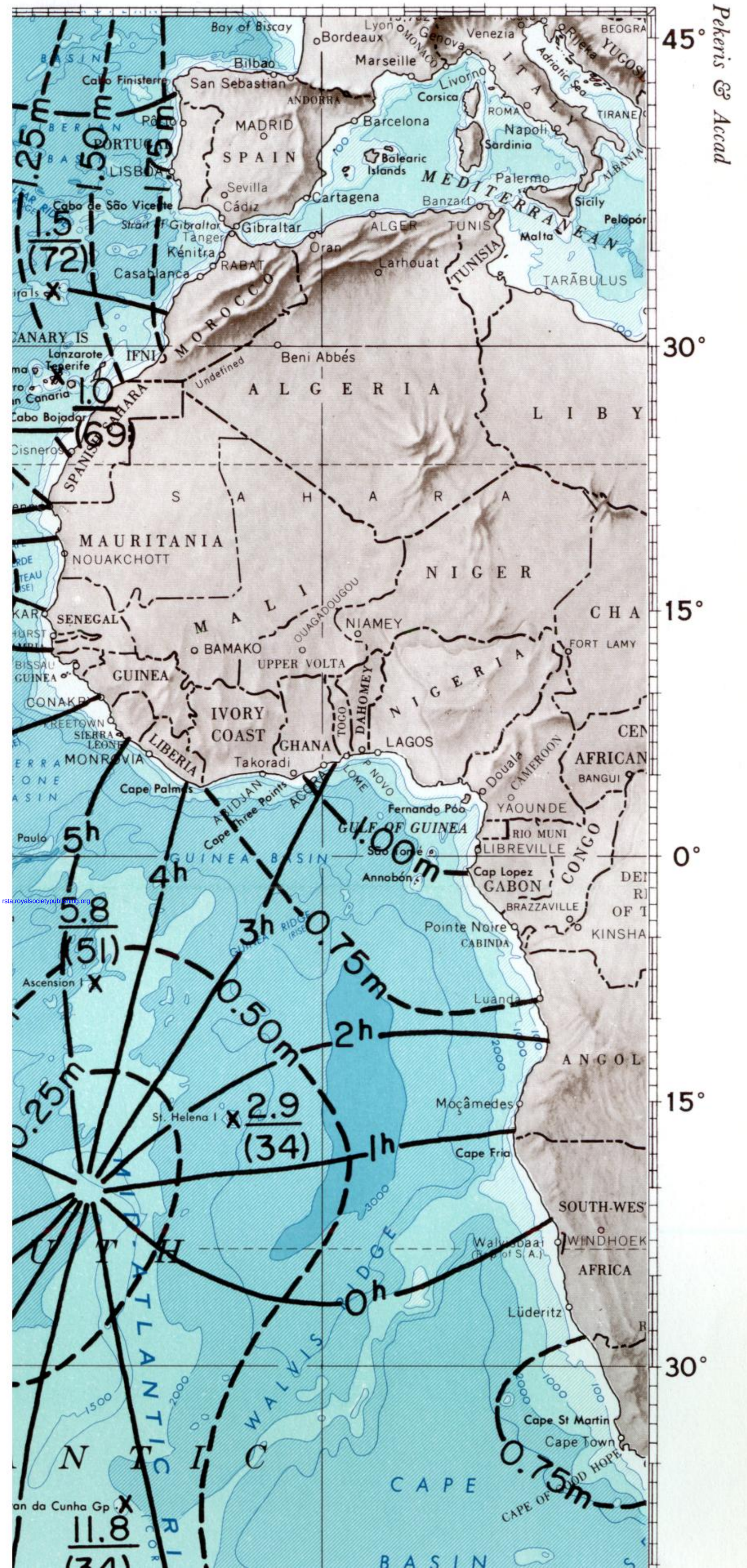

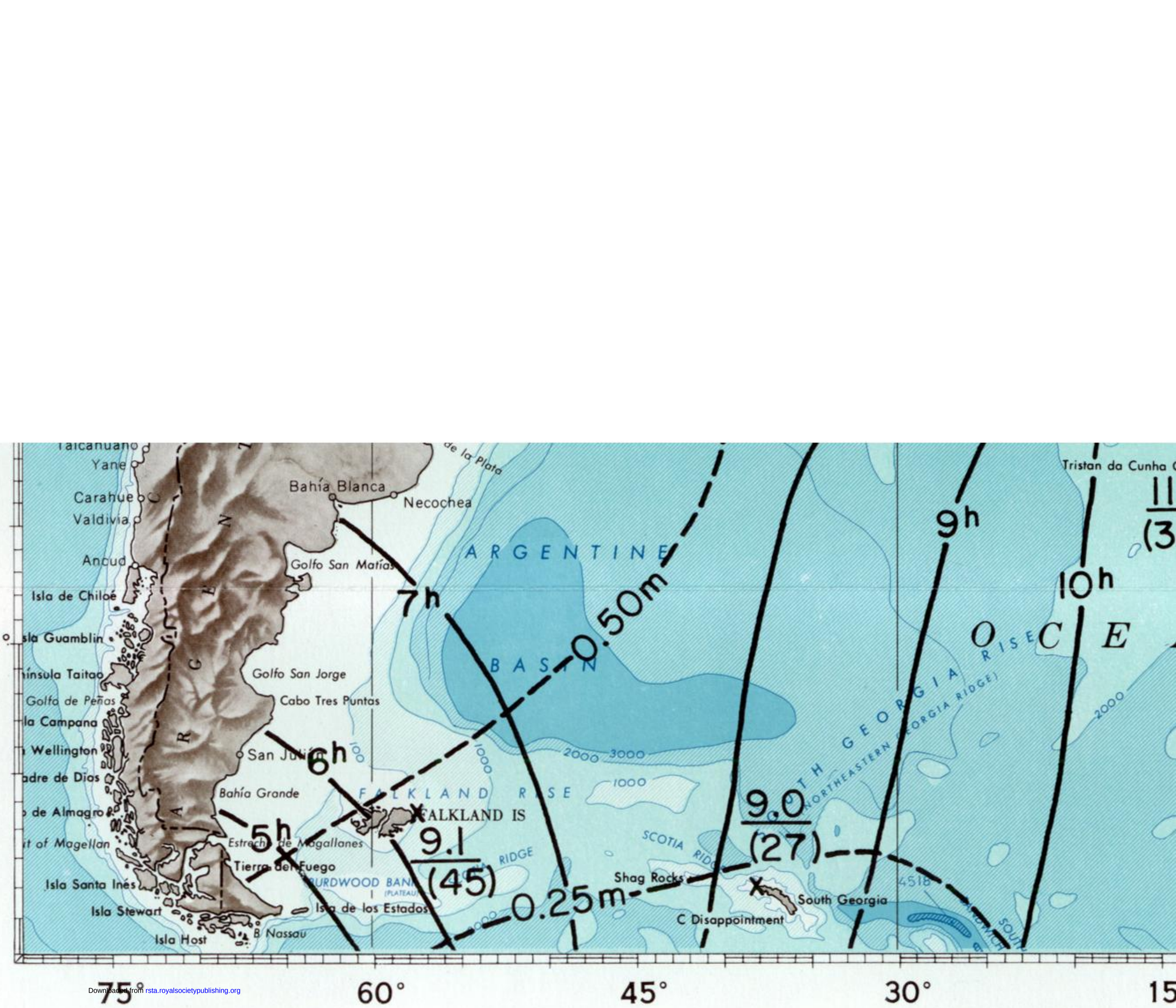

FIGURE 11. The Middle South Atlantic amphidrome (21 S, 15 W) for the M_2 ti
Underlined numbers give observed phase lags (in hours) of high tide, relative to th
Greenwich. Numbers in parentheses give the observed amplitudes in centimetres
lines; - - -, corange lines (in metres).

PHILOSOPHICAL TRANSACTIONS OF THE ROYAL SOCIETY A MATHEMATICAL, PHYSICAL & ENGINEERING SCIENCES

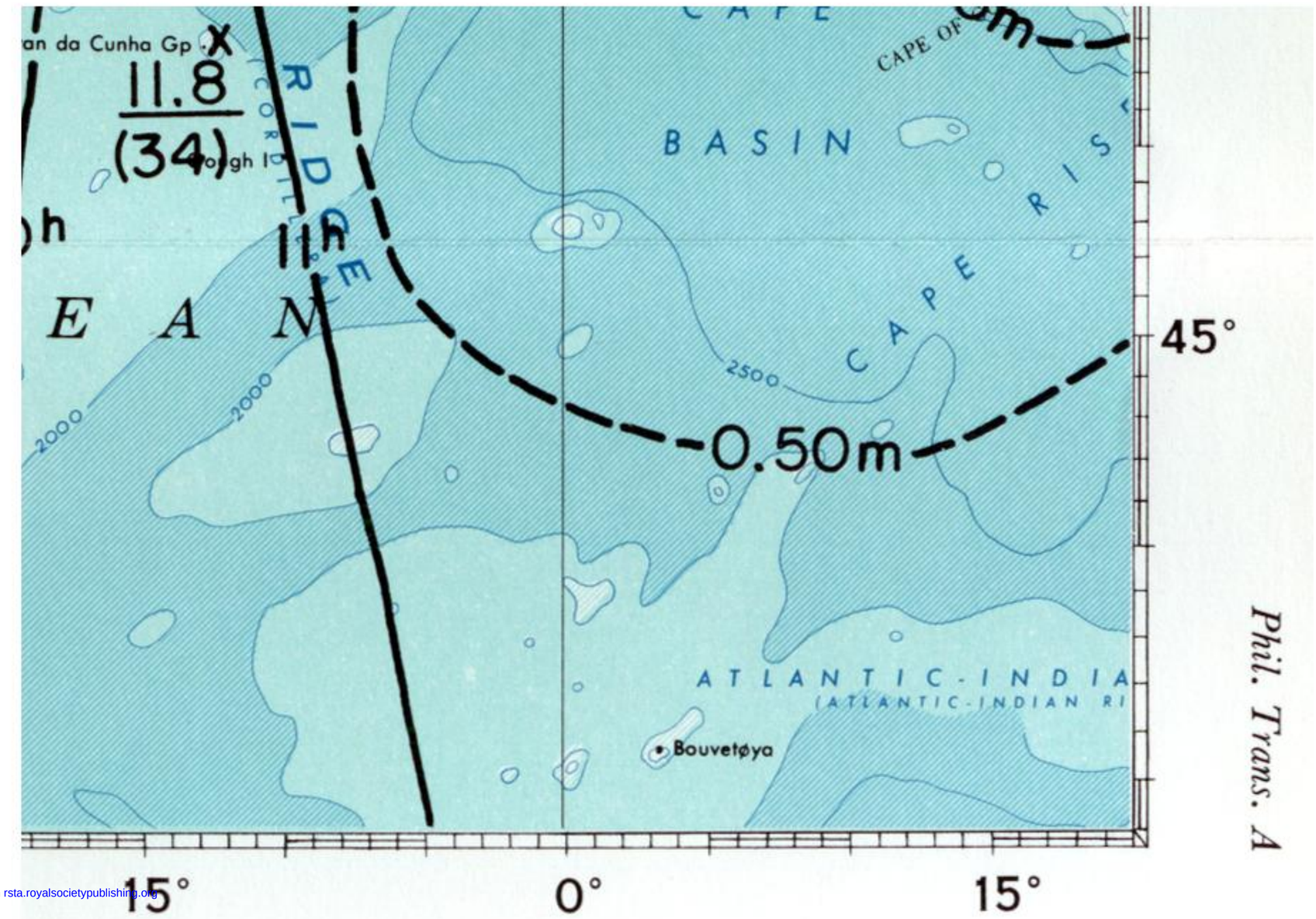

the M_2 tide, taken from figure 10.
ative to the time of lunar transit at
entimetres. ——, Theoretical cotidal